Article

Neuron

Local and Distant Input Controlling Excitation in Layer II of the Medial Entorhinal Cortex

Highlights

- LII MEC excitatory neurons can be classified into four cell types
- The four cell types exhibit specific local excitatory and inhibitory connectivity
- LII neurons contribute to the excitation of contralateral LII neurons
- Distinct septal GABAergic neurons exhibit cell-type-specific inhibition in LII MEC

Authors

Elke C. Fuchs, Angela Neitz, Roberta Pinna, Sarah Melzer, Antonio Caputi, Hannah Monyer

Correspondence

h.monyer@dkfz-heidelberg.de

In Brief

Medial entorhinal cortex comprises grid cells that play an important role in spatial navigation. Fuchs et al. characterized essential excitatory and inhibitory components of the underlying networks. This is a prerequisite to develop realistic models to explain grid cell activity.

Fuchs et al., 2016, Neuron *89*, 194–208
January 6, 2016
http://dx.doi.org/10.1016/j.neuron.2015.11.029

CellPress

CellPress

Neuron
Article

Local and Distant Input Controlling Excitation in Layer II of the Medial Entorhinal Cortex

Elke C. Fuchs,[1,2] Angela Neitz,[1,2] Roberta Pinna,[1,2] Sarah Melzer,[1,3] Antonio Caputi,[1] and Hannah Monyer[1,*]
[1]Department of Clinical Neurobiology, Medical Faculty of Heidelberg University and German Cancer Research Center (DKFZ), Im Neuenheimer Feld 280, 69120 Heidelberg, Germany
[2]Co-first author
[3]Present address: Department of Neurobiology, Howard Hughes Medical Institute, Harvard Medical School, 200 Longwood Avenue, WAB 347, Boston, MA 02115, USA
*Correspondence: h.monyer@dkfz-heidelberg.de
http://dx.doi.org/10.1016/j.neuron.2015.11.029

SUMMARY

Layer II (LII) of the medial entorhinal cortex (MEC) comprises grid cells that support spatial navigation. The firing pattern of grid cells might be explained by attractor dynamics in a network, which requires either direct excitatory connectivity between phase-specific grid cells or indirect coupling via interneurons. However, knowledge regarding local networks that support in vivo activity is incomplete. Here we identified essential components of LII networks in the MEC. We distinguished four types of excitatory neurons that exhibit cell-type-specific local excitatory and inhibitory connectivity. Furthermore, we found that LII neurons contribute to the excitation of contralateral neurons in the corresponding layer. Finally, we demonstrated that the medial septum controls excitation in the MEC via two subpopulations of long-range GABAergic neurons that target distinct interneurons in LII, thereby disinhibiting local circuits. We thus identified local connections that could support attractor dynamics and external inputs that likely govern excitation in LII.

INTRODUCTION

The medial entorhinal cortex (MEC) is a major in- and output structure of the hippocampus and participates in processes supporting spatial navigation, learning, and memory (Bannerman et al., 2001; Howard et al., 2014; Steffenach et al., 2005; Suh et al., 2011). The superficial layer II (LII) and layer III (LIII) of the MEC are the origin of the perforant path terminating in the dentate gyrus and the temporo-ammonic pathway directly targeting CA1 neurons in the hippocampus.

Neurons located in the superficial layers of the MEC exhibit distinct spatial firing patterns. The most extensively studied are LII/III grid cells, which display a hexagonal firing pattern in two-dimensional environments (Hafting et al., 2005). The increasing information pertaining to many of the unique grid cell features contrasts with the sparse knowledge regarding the generation of their conspicuous firing pattern. Many types of network models were proposed that try to account for the generation of grid-like firing (Burak, 2014; Burgess and O'Keefe, 2011; Giocomo et al., 2011; McNaughton et al., 2006). However, even promising attractor models have been recently challenged, as they are not fully supported by empirical data. Thus, an important premise of attractor models is based on the presence of local connectivity between grid cells. In earlier models, this was implemented by direct excitatory connections between grid cells. Alternatively, a grid cell pattern can emerge in networks based on purely inhibitory local connections (Burak and Fiete, 2009). Grid-like firing also was generated in attractor models with grid cell communication mediated disynaptically via inhibitory interneurons (Couey et al., 2013; Pastoll et al., 2013; Roudi and Moser, 2014). These models were supported by empirical data that showed a lack of connectivity between stellate cells (Dhillon and Jones, 2000), but bidirectional connectivity between stellate cells and local inhibitory neurons (Couey et al., 2013; Pastoll et al., 2013).

Although electrophysiological recordings in vitro failed to establish excitatory connections between stellate cells (i.e., putative grid cells), there is the intriguing possibility that other excitatory neurons in LII might support grid-like firing by providing local excitation, as required by attractor models based on excitatory recurrent connectivity. Indeed, electrophysiological in vivo data support this notion as, upon morphological reconstruction, putative grid cells were found to comprise both stellate and pyramidal neurons (Domnisoru et al., 2013). The idea that both cell types could exhibit a grid cell firing pattern, although to a different degree, received further support from experimental work in which juxtacellularly labeled putative grid cells (Tang et al., 2014) and in vivo Ca^{2+} imaging in distinct cell types (Sun et al., 2015) were analyzed. However, it is not clear whether, and to which extent, pyramidal cells are connected within LII.

On the basis of electrophysiological properties measured in vitro, Alonso and Klink (1993) identified the existence of two cell types in LII, namely stellate and pyramidal-like cells. These findings were further extended by Canto and Witter (2012), who also distinguished between stellate and pyramidal cells but pointed out that there is a certain degree of variability within each cell class. The presence of at least two defined types of

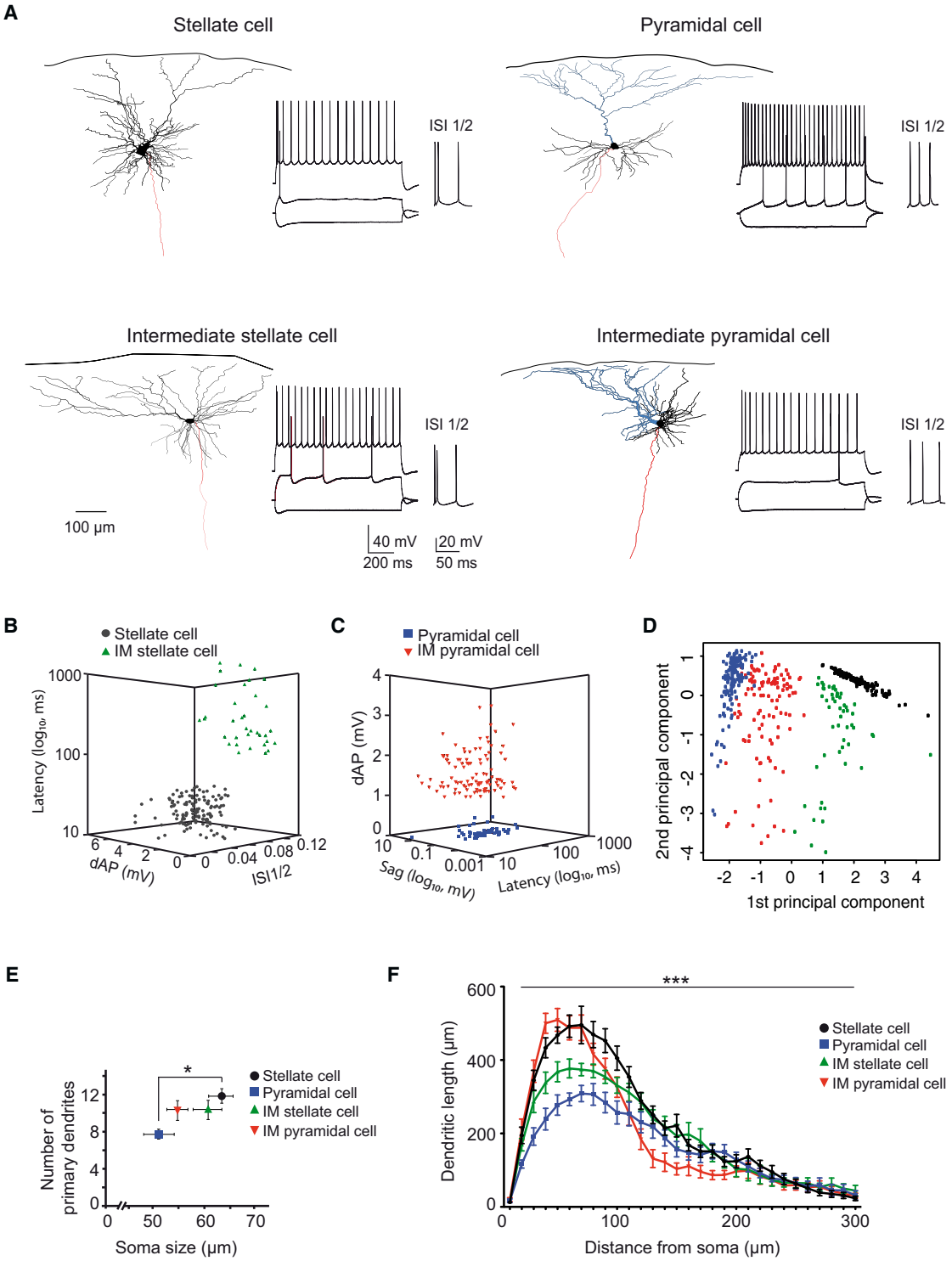

Figure 1. Morphological and Electrophysiological Features of Defined Excitatory LII Cell Types in Dorsal MEC

(A) Reconstruction of four representative neurons belonging to the indicated cell type (dendrites in black, apical dendrite in blue, axon in red) and their corresponding firing pattern upon somatic current injection (−200 to 600 pA). ISI1/2 plus dAP reveal differences between the four cell types: the stellate cell and intermediate stellate cell exhibit burstiness, the firing pattern of pyramidal cell and intermediate pyramidal cell displays adaptation, and dAP is absent in the pyramidal cell.

(B) Distribution of stellate (gray circles) and intermediate stellate cells (green triangles) when using latency to spike firing, ISI1/2, and dAP as distinction criteria.

(legend continued on next page)

excitatory neurons is further supported by immunohistochemical evidence. Thus, calbindin (CB) and reelin (RE) expression in LII was correlated with the pyramidal and stellate phenotype, respectively (Kitamura et al., 2014; Ray et al., 2014; Varga et al., 2010). Interestingly, the expression pattern of the two markers exhibited a striking modular organization (Kitamura et al., 2014; Ray et al., 2014).

There is indication that the two types of excitatory neurons are differentially wired both locally as well as with respect to their downstream targets. Thus, inhibition onto stellate cells is provided by fast-spiking (FS), parvalbumin-positive (PV^+) interneurons (Buetfering et al., 2014; Couey et al., 2013; Pastoll et al., 2013), while pyramidal cells are inhibited by cholecystokinin$^+$ interneurons (Varga et al., 2010). Regarding the output projections of the two cell types, there is clear evidence that stellate/RE^+ neurons constitute the perforant path and project to the dentate gyrus. The target area of pyramidal and/or CB^+ neurons is still an issue of debate. While Varga et al. (2010) reported that CB^+ neurons project to the contralateral MEC, a recent study proposed that CB^+/$WFS1^+$ neurons contribute to the temporo-ammonic pathway thereby directly targeting the CA1 region (Kitamura et al., 2014).

Finally, an important yet unresolved question pertains to the contribution of the external input in driving and/or modulating grid cell firing. Thus, inactivation of the medial septum (MS) disrupts the spatial periodicity of grid cell firing (Brandon et al., 2011; Koenig et al., 2011) without affecting the activity of other spatially tuned cells, such as boundary cells and head-direction cells. The septo-entorhinal pathway comprises cholinergic and GABAergic projections (Alonso and Köhler, 1984; Köhler et al., 1984). The latter received attention only lately. Thus, it is noteworthy that septal GABAergic neurons target FS and low threshold-spiking (LTS) interneurons in all layers of the MEC (Gonzalez-Sulser et al., 2014).

On the basis of these premises the following pressing questions arise: (1) Are pyramidal and/or CB^+ neurons in LII directly interconnected and can thereby support some of the demands requested by attractor network models? (2) Are there yet other excitatory cell types in LII, and if so, how are they locally connected? (3) Are excitatory LII neurons differentially connected to inhibitory LII neurons? (4) And finally, do other brain regions that project to the MEC (e.g. the septum or contralateral MEC) contribute substantially to the recruitment of LII neurons, and if so, what are the mechanisms by which they do so?

Hence we revisited the dorsal MEC and analyzed electrophysiological and morphological properties of LII MEC neurons. Aided by connectivity measurements performed in mice expressing fluorescent proteins in defined neurons, we distinguished distinct excitatory cell types that exhibit cell-type-specific excitatory and inhibitory local connectivity. We addressed the long-range connectivity by combining retrograde tracer injections with optogenetic and electrophysiological analysis of target neurons. We identified and characterized two external inputs, namely excitatory projections from the contralateral MEC and inhibitory projections from the MS.

RESULTS

Electrophysiological and Morphological Characterization of LII Excitatory Neurons

We identified four distinct types of excitatory neurons in LII, referred to hereafter as stellate cells, intermediate stellate cells, pyramidal cells, and intermediate pyramidal cells. Our classification is based on the following morphological and electrophysiological features: (1) hyperpolarizing and depolarizing sag potential, (2) burst firing (shorter ratio of ISI1/2) in response to depolarization, (3) depolarizing afterpotential (dAP), (4) latency to first spike, and (5) the presence of a main (apical) dendrite (Figure 1; Table S1). The first three criteria were used previously to differentiate between stellate and non-stellate cells in the MEC (Alonso and Klink, 1993; Canto and Witter, 2012). The most outstanding feature of stellate cells was the sag potential and burst firing, while pyramidal cells exhibited longer latency to first spike and more pronounced adaption of spike firing. In contrast to stellate cells, intermediate stellate cells displayed a significant longer latency to the first spike (>100 ms; Figures 1A and 1B; Table S1). Finally, the most prominent feature aiding in separating intermediate pyramidal cells from pyramidal cells was a clear dAP (>0.5 mV) in the former (Figures 1A and 1C; Table S1). Principal component analysis based on the five parameters resulted in a clear separation between stellate and pyramidal cells and underlined the ''intermediate'' distribution of the two intermediate cell types (Figure 1D).

A classification into four subtypes was further supported when morphological criteria were taken into account. Both the soma perimeter (63.38 ± 2.49 versus 51.18 ± 3.1 μm; $p < 0.05$) and number of primary dendrites (11.3 ± 0.8 versus 7.8 ± 0.59; $p < 0.05$, $n = 12$ and 8 cells, respectively; Figure 1E) were significantly different when comparing stellate cells and pyramidal cells. Values obtained for intermediate stellate and intermediate pyramidal cells were ''intermediate'' between those of stellate and pyramidal cells (soma perimeter: 60.72 ± 2.88 and 54.76 ± 2.16 μm; number

(C) Distribution of pyramidal cells (blue squares) and intermediate pyramidal cells (red triangles) when using dAP, sag potential, and latency as distinction criteria.

(D) Principal component analysis based on the same electrophysiological parameters as used in (B) and (C) plus the presence of an apical dendrite. The plot shows the first two principal components, with component 2 representing predominantly latency while component 1 combines information from the four remaining variables. Note the clear separation between stellate (black) and pyramidal cells (blue), whereas both intermediate cells (IM stellate [green] and IM pyramidal [red] cells) display an ''intermediate'' distribution.

(E) Differences in soma size and numbers of primary dendrites of the four excitatory cell types (*$p < 0.05$).

(F) Sholl analysis reveals difference between the four cell types when plotting dendritic length as a function of circular distance from the soma in 10-μm steps (two-way ANOVA, $F_{(144,1813)} = 4.43$, ***$p < 0.001$). Stellate and intermediate pyramidal cells exhibit locally (10–80 μm) a higher density of dendrites compared to pyramidal and intermediate stellate cells.

Abbreviations are as follows: ISI, interspike interval; dAP, depolarized afterpotential; and IM, intermediate. See also Figure S1 and Table S1.

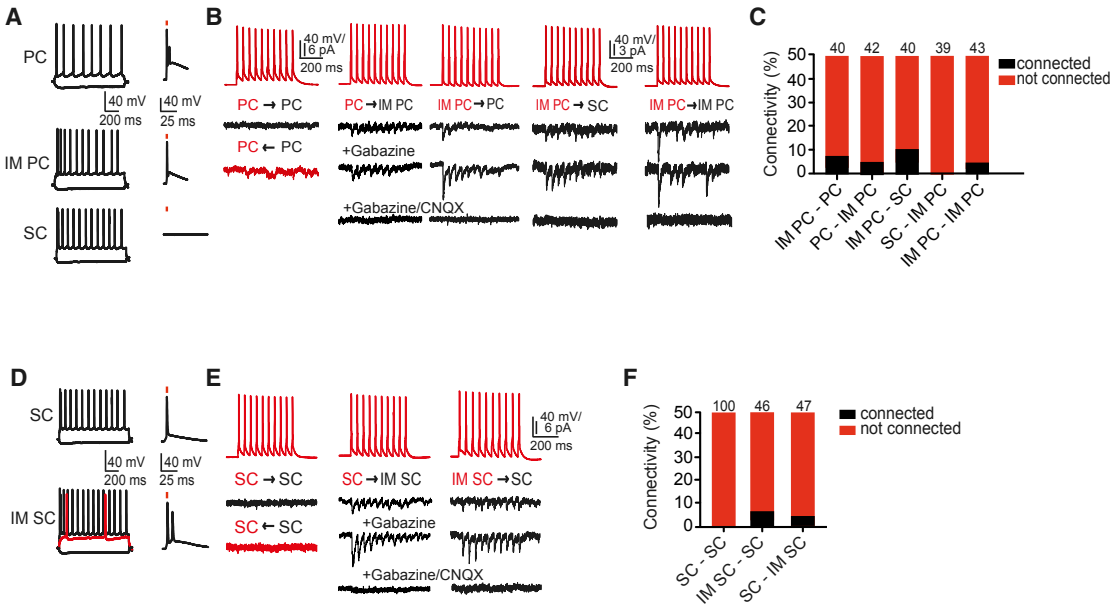

Figure 2. Local Excitatory Connectivity in LII of the MEC

(A) Firing pattern (left) of indicated excitatory cells in *CB*^{Cre} mice. The PC and IM PC, but not the SC, are excited by ChR2 stimulation (right, stimulation is indicated by red bar above the spike).

(B) uEPSCs recorded at −70 mV in indicated cells elicited by a train of 10 action potentials in the presynaptic neuron (40 Hz) (action potential traces in red, upper row). The direction of tested connectivity is indicated by an arrow. uEPSCs are not blocked by Gabazine, but by Gabazine plus CNQX (both at a concentration of 10 μM).

(C) Summary graph of investigated connections between indicated cell types.

(D) Firing pattern of tested excitatory cells in *Uchl1*^{Cre} mice. Representative examples showing activation of a SC and IM SC following ChR2 stimulation (stimulation is indicated by red bar above the spike).

(E) uEPSCs recorded at −70 mV in indicated cells elicited by a train of 10 action potentials in the presynaptic neuron (40 Hz) (action potential traces in red, upper row).

(F) Summary graph of investigated connections between indicated cell types. The numbers above the bars indicate the number of analyzed cell pairs.

Abbreviations are as follows: L, layer; IM, intermediate; MEC, medial entorhinal cortex; PC, pyramidal cell; SC, stellate cell; IM PC, intermediate pyramidal cell; and IM SC, intermediate stellate cell. See also Figures S2 and S3.

of primary dendrites: 10.4 ± 1.1and 10.3 ± 1.1, n = 10 and 12 cells, respectively; Figure 1E). Furthermore, Sholl analysis of reconstructed cells revealed a significant difference regarding the dendritic distribution between the four cell types (two-way ANOVA followed by post hoc Bonferroni test; Figure 1F; Figures S1A and S1B).

A classification of these four cell types based on morphological and physiological features had a less clear counterpart when the immunocytochemical markers RE and CB/WFS1 were employed. Even though RE was expressed in all stellate cells and intermediate stellate cells, the marker could be detected also to a variable extent in cells belonging to the other two cell types. Similarly, WFS1 was detected in a large proportion of pyramidal cells and intermediate pyramidal cells, but the marker could be found also in some intermediate stellate cells (Table S1). On the basis of marker expression a defined cell type could not be further subdivided. In other words, the electrophysiological properties of intermediate pyramidal cells expressing RE did not differ from those of intermediate pyramidal cells expressing WFS1. In our hands, WFS1 was a more reliable marker than CB in post hoc analysis of biocytin-filled cells. The two markers colocalized almost completely in LII excitatory cells of dorsal MEC (97.9% ± 0.7% of 934 CB$^+$/GAD67^{EGFP-} neurons counted in 4 hemispheres from 2 *GAD67*^{EGFP} mice).

Local Connectivity between Distinct Excitatory LII Neurons

As CB is preferentially expressed in pyramidal and intermediate pyramidal cells and RE marks stellate and intermediate stellate cells, we employed mice in which CB$^+$ and RE$^+$ neurons were fluorescently labeled to speed up the identification of excitatory neurons when measuring their putative connectivity (Figure S2).

To identify CB$^+$ neurons, we injected adeno-associated viral vector (AAV) DIO ChR2-mCherry into the MEC of *CB*^{Cre} mice. This resulted in specific mCherry expression in CB$^+$ neurons (Figures S2A–S2D) that, based on their firing pattern, could be easily further classified as pyramidal and intermediate pyramidal cells (Figure 2A). Non-labeled neurons comprised stellate and intermediate stellate cells. We recorded unitary excitatory postsynaptic currents (uEPSCs) from pairs of neurons whose somata were located at a distance of <40 μm in LII. We elicited trains of presynaptic action potentials (10 spikes at 40 Hz), and searched in neighboring neurons for monosynaptic uEPSCs that were sensitive to the AMPA receptor inhibitor CNQX, but

not to the $GABA_A$ receptor antagonist Gabazine. Direct connections between pairs of pyramidal cells or between pyramidal cells and stellate cells were extremely rare (1 of 56 pyramidal-pyramidal pairs, and 0 of 38 pyramidal-stellate pairs; Figures S3A and S3B). In contrast, intermediate pyramidal cells excited both pyramidal and stellate cells with higher probability (Figures 2A–2C; Figures S3A and S3B). Thus, the connectivity from intermediate pyramidal cells to pyramidal cells was 7.5% (3 of 40 pairs), and 4.8% in the opposite direction (2 of 42 pairs; Figures 2A–2C; Figures S3A and S3B). In pairs of intermediate pyramidal cells and stellate cells, the connectivity was 10.0% from intermediate pyramidal cells to stellate cells (4 of 40 pairs), but absent in the opposite direction (0 of 39 pairs; Figures 2A–2C; Figures S3A and S3B). Between intermediate pyramidal cell pairs, the connectivity was 4.7% (2 of 43 pairs; Figures 2A–2C; Figures S3A and S3B).

To aid the identification and study the two predominantly RE expressing cell types, namely stellate and intermediate stellate cells, we injected AAV DIO ChR2-mCherry into the MEC of *Uchl1*^{Cre} mice, which resulted in fluorescently labeled RE^+ neurons (Figures S2E and S2F). We concur with previous observations (Couey et al., 2013) that stellate cells (classified based on electrophysiological parameters) are not connected (0 of 100 pairs tested in both directions). However, the connectivity between intermediate stellate cells and stellate cells was 6.5% (3 of 46 pairs), and 4.3% in the opposite direction (2 of 47 pairs; Figures 2D–2F; Figures S3C and S3D).

Local Connectivity between Distinct Excitatory and Inhibitory LII Neurons

To test whether the four excitatory cell types in LII differ with respect to their inhibitory input, we recorded from pairs of excitatory cells and neighboring inhibitory neurons belonging to one of the three major interneuron subpopulations, namely PV^+, somatostatin$^+$ (SOM), and 5-HT_{3A}^+ neurons (Lee et al., 2010).

FS putative PV^+ interneurons were reported to provide extensive inhibition onto stellate cells (Beed et al., 2013; Couey et al., 2013). PV immunohistochemistry, however, indicates that CB^+/$WFS1^+$ neurons must also be targeted by PV^+ interneurons as evidenced by basket-like structures around CB^+/$WFS1^+$ cell bodies (Figures 3A and 3B; Figures S4A–S4C). To probe for the presence of monosynaptic connectivity between FS interneurons and all four excitatory cell types, we performed paired recordings in neurons identified by their firing pattern. We recorded unitary inhibitory PSCs (uIPSCs) at a holding potential of −50 mV in excitatory cells, and uEPSCs at −70 mV in FS interneurons, respectively. In agreement with previous data (Couey et al., 2013), connectivity from FS interneurons onto stellate cells was 35.7% (10 of 28 pairs), and 25.9% in the opposite direction (7 of 27 pairs; Figure 3C; Figure S5A). There was no connectivity in either direction between FS interneurons and pyramidal cells (0 of 29 pairs for each direction). Notably, FS interneurons inhibit both intermediate pyramidal cells and intermediate stellate cells, and receive excitatory input from both. Thus, in pairs of FS interneurons and intermediate pyramidal cells, the probability of monosynaptic uIPSCs was 36.6% (15 of 41 pairs), and that of uEPSC 47.5% (19 of 40 pairs; Figure 3C; Figure S5A). Connectivity from FS interneurons to intermediate stellate cells was 45.5% (10 of 22 pairs), and 28.6% (6 of 21 pairs) in the opposite direction (Figure 3C; Figure S5A).

SOM^+ and PV^+ interneurons are virtually non-overlapping cell populations as revealed by double-labeling experiments upon injection of AAV DIO ChR2-mCherry into the MEC of *SOM*^{Cre} mice (Figure 3D**)**. Also the axonal targeting pattern differed between the two interneuron populations. Thus, SOM^+ axons extended preferentially between islands and in LI (Figure 3E). The firing pattern of all virally transduced fluorescent SOM^+ interneurons was characterized by low-threshold firing and the presence of a prominent sag potential (Figure 3F; Figure S5B). In pairs of SOM^+ interneurons and excitatory cells, we detected inhibitory input onto stellate cells and intermediate pyramidal cells (5 of 37 tested SOM^+-stellate cell pairs, 5 of 41 tested SOM^+-intermediate pyramidal cell pairs; Figure 3F; Figure S5B). In contrast, pyramidal cells and intermediate stellate cells received no monosynaptic uIPSCs from SOM^+ interneurons (0 of 40 tested SOM^+-pyramidal cell pairs, 0 of 25 SOM^+-intermediate stellate cell pairs; Figure 3F; Figure S5B). Excitation onto SOM^+ cells was provided by stellate cells (5 of 35 pairs), intermediate pyramidal cells (12 of 41 pairs), and intermediate stellate cells (2 of 21 pairs), but not pyramidal cells (0 of 41 pairs).

5-HT_{3A}^+ interneurons, identified with the help of *5-HT*$_{3A}^{EGFP}$ mice (Inta et al., 2008), constituted the third discrete interneuron cell population in LII of the MEC (Figures 3G and 3H), as reported for somatosensory cortex (Lee et al., 2010). The firing patterns of this interneuron cell population were reminiscent of what was found in the somatosensory cortex (Lee et al., 2010). We detected inhibitory monosynaptic input from 5-HT_{3A}^{EGFP+} interneurons onto all four excitatory cell types, with the preferred target being intermediate pyramidal cells and pyramidal cells (Figure 3I). Thus, the connectivity from 5-HT_{3A}^{EGFP+} interneurons to pyramidal cells was 26.3% (10 of 38 pairs), and that from 5-HT_{3A}^{EGFP+} interneurons to intermediate pyramidal cells 25.0% (10 of 40 pairs; Figure 3I; Figure S5C). Finally, 5-HT_{3A}^{EGFP+} interneurons received excitation from all four cell types, that is, stellate cells (1 of 44 pairs), pyramidal cells (3 of 46 pairs), intermediate pyramidal cells (5 of 35 pairs), and intermediate stellate cells (2 of 31 pairs).

CB^+ Neurons Are a Source of Excitation to LII Neurons in the Contralateral MEC

Varga et al. (2010) reported that CB^+ neurons in LII project to the contralateral MEC. Two recent studies emphasized that CB^+ neurons are organized in islands (Kitamura et al., 2014; Ray et al., 2014). Hence the following question was raised: Are CB^+ neurons in islands the main source connecting the left and right MEC? We injected unilaterally the retrograde tracer cholera toxin subunit B (CTB) into the MEC of wild-type mice. Indeed, we could detect CTB^+ neurons in LII of the contralateral MEC (Figure 4A). To further verify their identity, we performed immunohistochemical experiments. We found that 76.9% ± 2.8% CTB^+ LII neurons were CB^+ (626 CTB^+ neurons in 5 hemispheres from 5 wild-type mice) and RE^- (only 1% ± 0.6% was RE^+, 384 CTB^+ neurons in 5 hemispheres from 5 wild-type mice). Most CTB^+/CB^+ LII neurons (89.5% ± 1.6%) were localized in CB islands (Figure 4B). In deep LII, CTB^+/CB^+ neurons displayed a typical pyramidal-cell-like morphology, in contrast to more superficially

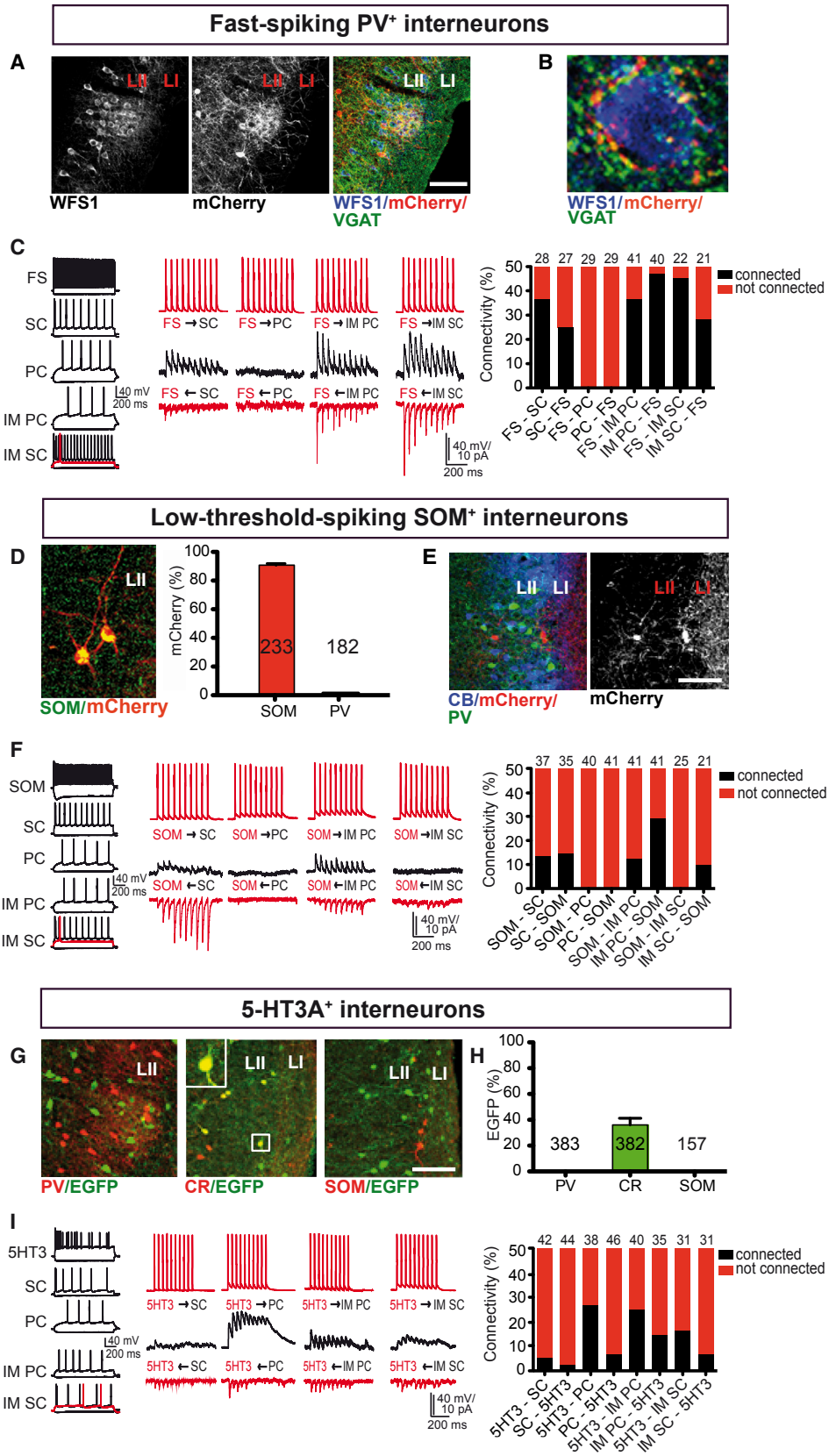

(legend on next page)

localized CTB$^+$/CB$^+$ neurons that exhibited an oblique orientation of their soma and apical dendritic tree (Figure 1A; Figure S6), reminiscent of the previously described oblique pyramidal cells (Canto and Witter, 2012; Klink and Alonso, 1997). On the basis of electrophysiological properties, we classified the former CTB$^+$ cells as pyramidal cells (Figure 1A) and the latter as intermediate pyramidal cells (Figure 1A). It should be pointed out though that the majority of CTB$^+$ neurons were located in LIII (Figure 4A).

To probe whether the interhemispheric MEC connectivity comprises also a GABAergic component, CTB was injected unilaterally into the MEC of *GAD67*^{EGFP} mice. We did not detect retrogradely labeled GABAergic neurons (LII: 443 CTB$^+$/GAD67$^-$ neurons; LIII: 1790 CTB$^+$/GAD67$^-$ neurons, 3 hemispheres from 3 *GAD67*^{EGFP} mice).

To detect target neurons of the contralaterally projecting CB$^+$ neurons, we injected AAV DIO-ChR2-mCherry unilaterally into the MEC of *CB*^{Cre} mice (Figure 4C) and investigated the axonal projection pattern in the contralateral MEC (n = 3 mice; Figure 4D). Fluorescently labeled axons targeted LII and LI (Figure 4D).

To identify target neurons in LII of the contralateral MEC, we combined laser stimulation of ChR2-expressing axons and whole-cell recordings. Laser stimulation elicited reliable EPSCs in stellate, intermediate stellate, and FS cells, and less frequently in pyramidal and intermediate pyramidal cells and non-FS interneurons (Figure 4E; Table S2). To distinguish between direct (monosynaptic) and indirect (polysynaptic) responses, we blocked voltage-dependent Na$^+$ channels with 1 μM tetrodotoxin (TTX), and K$^+$ channels that are critical for axonal repolarization with 100 μM 4-aminopyridin (4-AP). We detected monosynaptic input from the contralateral MEC in stellate cells, intermediate stellate cells, and FS interneurons. The excitatory nature of the connections was further substantiated by the selective blockage with 10 μM CNQX and 50 μM D-AP5, but not with 10 μM Gabazine (n = 6 cells; Figure 4E; Table S2).

Excitatory and Inhibitory LII Neurons Project to the MS

Given that injection of the retrograde tracer CTB into the contralateral MEC always led to the labeling of a small fraction of CB$^+$ neurons within an island, we wondered whether CB$^+$ neurons might also project to other brain areas. We chose to first investigate the MS as this structure is reciprocally connected with the MEC (Alonso and Köhler, 1984). Upon injection of CTB into the MS of *GAD67*^{EGFP} mice, we detected labeled LII neurons that were often clustered (Figure 5A). Staining with CB or RE antibodies revealed that most CTB$^+$ cells were excitatory CB$^+$/GAD67$^-$ neurons (69% ± 2.2% CTB$^+$/CB$^+$/GAD67$^-$; of these, 92.7% ± 1.8% CTB$^+$/CB$^+$/GAD67$^-$ were localized in CB islands; a total of 449 CTB$^+$ neurons in 8 hemispheres from 4 *GAD67*^{EGFP} mice were analyzed; Figure 5B). In addition, electrophysiological characterization indicated that all tested CTB$^+$ cells exhibited an intermediate pyramidal cell phenotype (6 out of 6 cells from 3 mice). We detected a small population of RE$^+$ cells that also project to the MS (6.3% ± 2.4% CTB$^+$/RE$^+$/GAD67$^-$; 225 CTB$^+$ neurons in 5 hemispheres from 3 *GAD67*^{EGFP} mice; Figure 5B). These neurons were localized in the intermediate or ventral MEC.

We subsequently investigated whether a defined island provides input to both the contralateral MEC and the MS. To this end we injected green fluorescently labeled CTB into the MS and red fluorescently labeled CTB into the contralateral MEC. Notably, we could detect the two fluorochromes in CB$^+$ neurons that were localized within the same island (n = 4 wild-type mice; Figure 5C).

Interestingly, CTB injection into the MS of *GAD67*^{EGFP} mice revealed the existence not only of excitatory CTB$^+$/EGFP$^-$ neurons

Figure 3. Local Inhibitory Connectivity in LII of the MEC

(A) WFS1$^+$ neurons in an island (left) receive innervation from PV$^+$ axons visualized by mCherry expression following AAV DIO ChR2-mCherry injection into the MEC of a *PV*^{Cre} mouse (middle). The merged picture shows immunostaining for VGAT, a marker of GABAergic terminals (right). Scale bar, 100 μm.

(B) Confocal image of PV$^+$ and VGAT$^+$ axon terminals surrounding the soma of a WFS1$^+$ neuron in LII.

(C) Firing pattern (left) and representative traces (middle) of unitary IPSCs (uIPSCs, black) and unitary EPSCs (uEPSCs, red) recorded in FS interneurons and excitatory cells. uIPSCs were recorded at −50 mV, and uEPSCs at −70 mV in the respective postsynaptic neuron, and were elicited by a train of 10 action potentials (40 Hz) (train of 10 action potentials in red). The summary graph (right) shows the investigated connections between LII FS interneurons and excitatory cells.

(D) MCherry expression in SOM$^+$ interneurons in LII following AAV DIO ChR2-mCherry injection into the MEC of a *SOM*^{Cre} mouse (left). Quantification of mCherry$^+$ interneurons that expressed SOM or PV in MEC LII of *SOM*^{Cre} mice (right). The numbers indicate analyzed mCherry$^+$ neurons from two mice.

(E) PV$^+$ and SOM$^+$ (labeled by mCherry following AAV DIO ChR2-mCherry injection into the MEC of a *SOM*^{Cre} mouse) interneurons in LII are localized preferentially around islands (left). mCherry expression reveals that fluorescently labeled axons of SOM$^+$ interneurons are localized between islands and in LI (right). Scale bar, 100 μm.

(F) Firing pattern (left) and representative traces (middle) of uIPSCs (black) and uEPSCs (red) recorded in SOM$^+$ interneurons and excitatory cells. Connectivity was tested by eliciting a train of 10 action potentials in the presynaptic neuron (train of action potentials in red). The summary graph (right) shows the quantitative evaluation of connectivity between SOM$^+$ interneurons and indicated excitatory cells.

(G) PV (left), calretinin (middle), and SOM (right) immunostaining in MEC LII of a *5-HT*$_{3A}^{EGFP}$ mouse. The boxed double-labeled CR$^+$/EGFP$^+$ interneuron is shown at a higher magnification in the upper left corner. Scale bar, 100 μm.

(H) Quantification of EGFP$^+$ interneurons expressing PV, CR, or SOM in LII of the MEC in *5-HT*$_{3A}^{EGFP}$ mice. The numbers indicate analyzed EGFP$^+$ neurons from two or three mice.

(I) Firing pattern (left) and representative traces (middle) of uIPSCs (black) and uEPSCs (red) detected in 5-HT$_{3A}^{EGFP+}$ interneurons and excitatory cells. The summary graph (right) shows quantitative evaluation of investigated connections between indicated cell types. Data are represented as percentage of analyzed connections. The total number for the different cell pairs is indicated above the bars.

Abbreviations are as follows: PC, pyramidal cell; SC, stellate cell; IM PC, intermediate pyramidal cell; IM SC, intermediate stellate cell; CR, calretinin; 5-HT$_{3A}$, 5-HT$_{3A}$ receptor; 5HT3, 5-HT$_{3A}^+$ interneuron; L, layer; PV, parvalbumin; SOM, somatostatin; and VGAT, vesicular glutamate transporter. See also Figures S4 and S5.

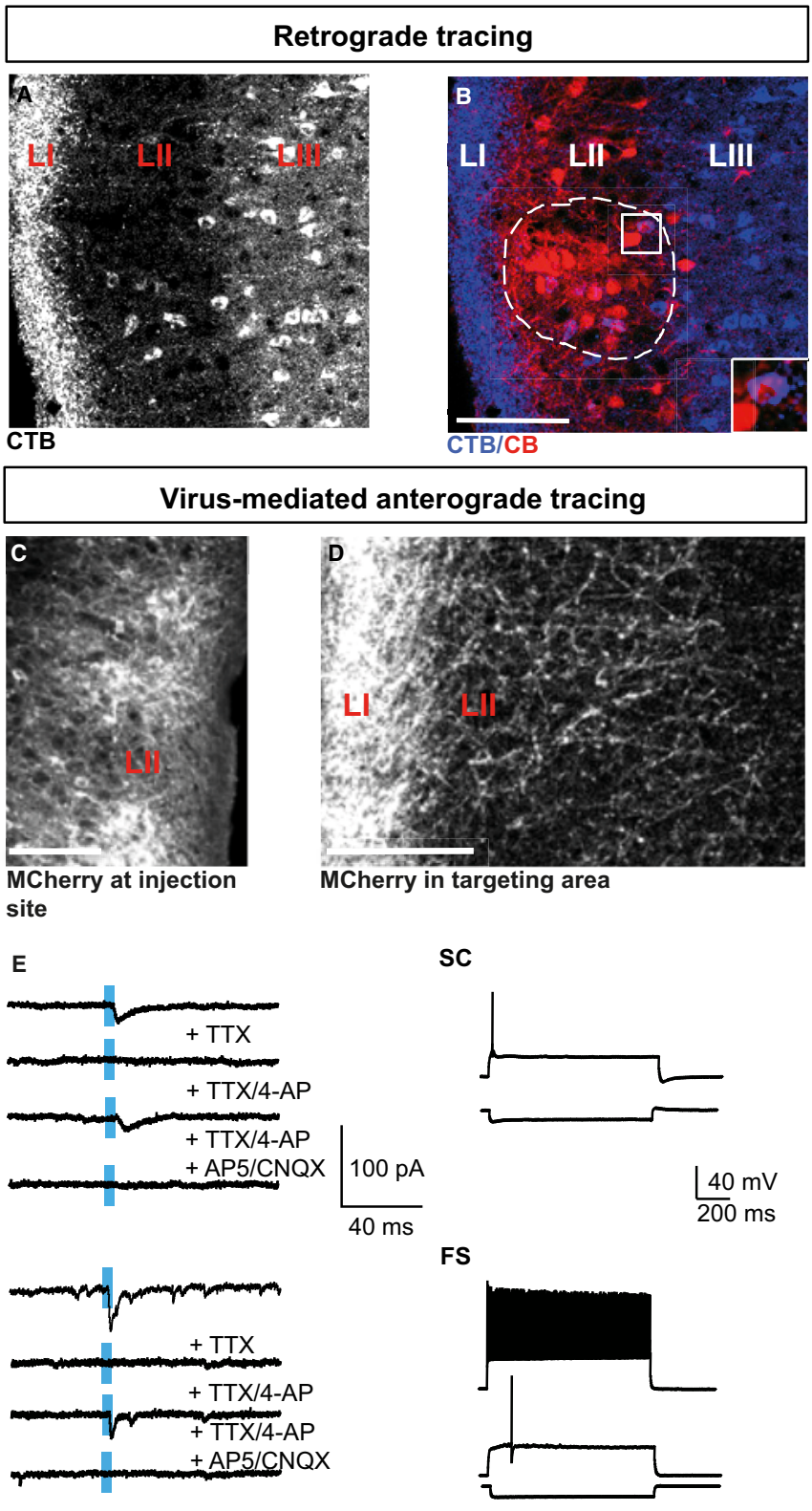

Figure 4. LII CB$^+$ Neurons Target Multiple Cell Types in LII of the Contralateral MEC

(A) Retrogradely labeled LII and LIII neurons following CTB injection into the contralateral MEC (sagittal section).

(B) Most retrogradely labeled neurons (blue) in LII were CB$^+$ (red) and localized in CB$^+$ islands (the confines of this island are indicated by a dashed line). The Inset is a higher magnification of the indicated area (white square) and shows a CTB$^+$/CB$^+$ neuron. Scale bar, 100 μm.

(C) Confocal image of injection site in LII following AAV DIO-ChR2-mCherry injection into the MEC of *CB*^{Cre} mice. Scale bar, 100 μm.

(D) Sagittal MEC section showing innervation of LII following AAV DIO-ChR2-mCherry injection into the contralateral MEC of *CB*^{Cre} mice. Scale bar, 100 μm.

(E) Synaptic responses and firing pattern of a targeted SC and a FS interneuron. ChR2-mCherry-expressing axons were stimulated by 5-ms laser pulses (blue bar) and EPSCs were recorded. Excitatory and monosynaptic inputs were identified in the presence of the indicated antagonists.

Abbreviations are as follows: L, layer; CTB, cholera toxin subunit B; MEC, medial entorhinal cortex; FS, fast-spiking interneuron; and SC, stellate cell. See also Figure S6 and Table S2.

in LII of the MEC but also of CTB$^+$/EGFP$^+$ cells, pointing to the presence of long-range GABAergic neurons in the MEC that project to the MS (6.1% ± 2.8% CTB$^+$/GAD67$^+$; a total of 449 CTB$^+$ neurons in 8 hemispheres from 4 *GAD67*^{EGFP} mice were analyzed; Figure 5D).

Distinct Populations of GABAergic Neurons from the MS Target the MEC

There is evidence that interareal connectivity via long-range GABAergic projections is often reciprocal (Caputi et al., 2013). Hence we injected the retrograde tracer fluorogold (FG) into the MEC of wild-type mice and detected FG$^+$ neurons that were distributed throughout the dorsal-ventral extent of the MS (Figures 6A and 6B). Concomitant labeling with GABAergic neuron markers revealed PV$^+$ neurons in the MS as one source for long-range GABAergic projections to the MEC (9.9% ± 4.7% FG$^+$/PV$^+$; 663 FG$^+$ neurons in 4 wild-type mice; Figure 6A). We also identified retrogradely labeled CB$^+$ neurons, providing evidence that more than one GABAergic subpopulation of the MS projects to the MEC (7.7% ± 0.6% FG$^+$/CB$^+$; 526 FG$^+$ neurons in 4 wild-type mice; Figure 6B).

Following injections of FG into the right hippocampus and CTB into the right MEC of the same mouse, we identified PV$^+$ and CB$^+$ neurons labeled with both retrograde tracers, suggesting that

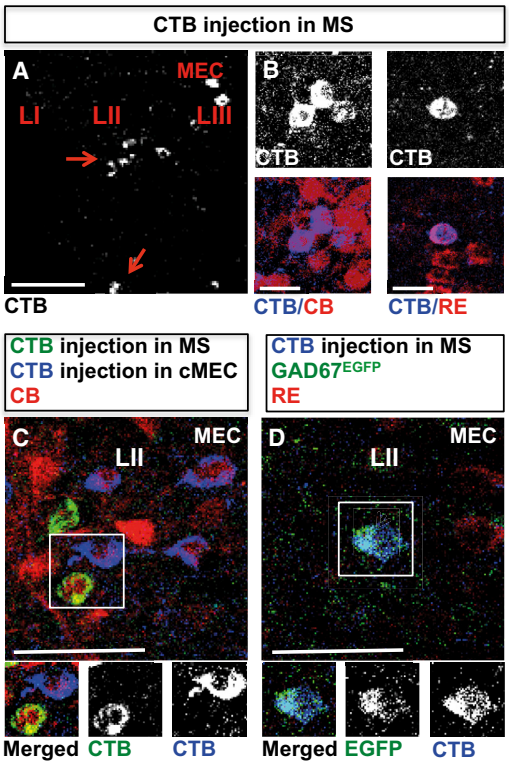

Figure 5. LII Neurons Project to the MS

(A) CTB^+ neurons in MEC LII (red arrows) following tracer injection into the MS. Scale bar, 100 μm.

(B) CTB^+/CB^+ neurons located in CB islands (left two panels) and CTB^+/RE^+ cells (right two panels) following CTB injection into the MS. Scale bars, 20 μm.

(C) CB^+ neurons (red) located in the same CB island can project to either the MS (green CTB labeling) or the contralateral MEC (blue CTB labeling). Boxed double-labeled neurons are shown below as a merged image and the single channel for green and blue CTB. Scale bar, 50 μm.

(D) *GAD67*$^{EGFP+}$ neuron in LII co-labeled with CTB following tracer injection into the MS (upper panel). The boxed double-labeled neuron is shown below as a merged image and the single channel for EGFP and blue CTB. Scale bar, 50 μm.

Abbreviations are as follows: CB, calbindin; c, contralateral; CTB, cholera toxin subunit B; L, layer; MEC, medial entorhinal cortex; MS, medial septum; and RE, reelin.

single GABAergic neurons in the MS can project to both target regions (7 $FG^+/CTB^+/PV^+$ neurons in 3 mice, 430 FG^+ and 107 CTB^+ neurons; 3 $FG^+/CTB^+/CB^+$ cells in 2 mice, 248 FG^+ and 53 CTB^+ neurons; Figures 6C and 6D).

GABAergic Long-Range Neurons Originating in the MS Target Distinct Inhibitory Neurons in LII

After establishing that PV^+ and CB^+ neurons originating in the MS project to the MEC, we next sought to determine the identity of the target cells. To this end we first injected AAV DIO ChR2-mCherry into the MS of *PV*^{Cre} mice. Virus injection resulted in specific expression of the fluorescent fusion protein ChR2-mCherry in PV^+ neurons of the MS (Figure 7A). In the MEC, the projections of these neurons could be detected throughout all layers. MCherry-labeled axons formed a dense network in LII (Figure 7B). The GABAergic phenotype of the long-range axons was confirmed by their VGAT positivity (data not shown).

Subsequently we combined laser stimulation of ChR2-positive axons with patch-clamp recordings and morphological reconstruction of target cells in MEC LII. Despite the dense axonal plexus, none of the glutamatergic neurons belonging to the four cell types described above—stellate cells, intermediate stellate cells, pyramidal cells, and intermediate pyramidal cells—responded to laser stimulation (n = 99 cells from 19 mice; Figure 7D). Responses could be detected only in GABAergic neurons (Figures 7C and 7D). Target cells comprised both FS and non-FS GABAergic neurons. Of the analyzed FS cells, two-thirds responded to laser stimulation (66% out of 53 cells from 17 mice; Figures 7D and 7E), whereas only one-third of non-FS GABAergic neurons responded (32% out of 28 cells from 10 mice; Figures 7D and 7E). The GABAergic nature of responses was confirmed by the reversal potential (−59.5 ± 2.1 mV, n = 8 cells from 5 mice) and the blockage with Gabazine, but not with D-AP5 and CNQX (n = 7 out of 7 cells from 6 mice; Figure 7C). Similar results were obtained following viral infection of septal glutamatergic and GABAergic neurons. All recorded responses in LII were restricted to GABAergic interneurons and were inhibitory (Figure S7).

We tested how inhibition via PV^+ long-range projections affected the activity of targeted FS neurons. We depolarized responding FS cells to suprathreshold potentials and activated long-range axons locally with 8-Hz laser pulses of 60-ms duration to simulate rhythmic burst firing of PV^+ cells in the MS (Borhegyi et al., 2004; King et al., 1998; Li et al., 2014). All analyzed FS neurons in MEC LII reduced their firing rate during laser stimulation transiently (n = 11 cells from 5 mice; Figure 7F). The overall firing rate was reduced from 10.2 ± 1.1 Hz to 6.8 ± 0.9 Hz during laser stimulation ($p < 0.01$, repeated-measures ANOVA followed by post hoc Tukey's test), while no persistent changes of the post-stimulation firing rate were seen ($p > 0.05$, repeated-measures ANOVA followed by post hoc Tukey's test).

To determine the targets of septal long-range CB^+ neurons, we injected AAV DIO ChR2-mCherry into the MS of *CB*^{Cre} mice. Virus injection resulted in specific expression of the fluorescent fusion protein ChR2-mCherry in CB^+ neurons of the MS (Figure S8A). In the MEC, mCherry-labeled axons reached LII, and the GABAergic phenotype of the long-range axons was confirmed by their VGAT positivity that was visible in the transition zone between LI and LII (Figure S8B). Of note, responses could be detected only in LTS interneurons (80% out of 30 cells from 9 mice; Figure S8C).

DISCUSSION

Local Excitatory and Inhibitory Network in LII

On the basis of electrophysiological parameters, we distinguished in addition to stellate and pyramidal cells two other excitatory cell types in LII, namely intermediate stellate and intermediate pyramidal cells. When scrutinizing previous studies, a certain extent of heterogeneity within the two cell classes can be inferred. Thus, in the study by Klink and Alonso (1997), both electrophysiologically identified stellate and pyramidal neurons exhibit some variability with respect to their morphology. Further

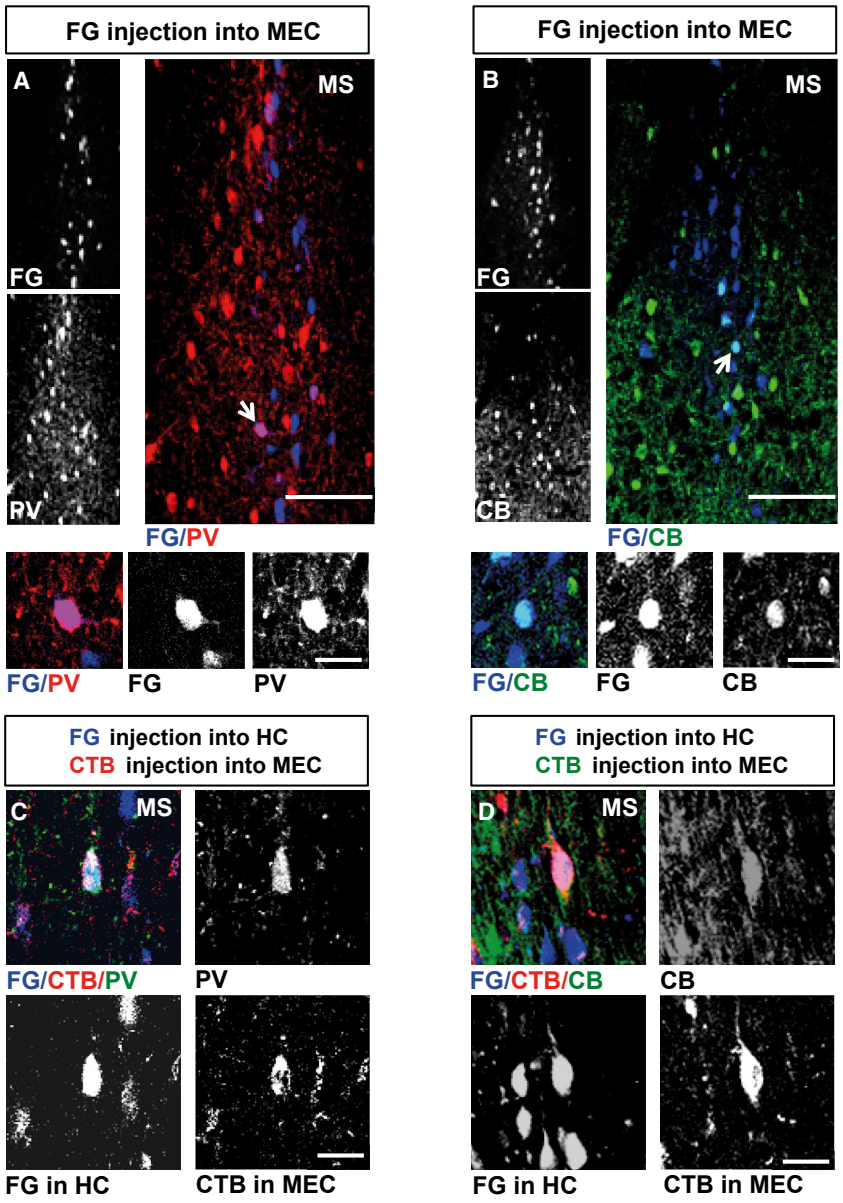

Figure 6. Septal GABAergic Neurons Projecting to the MEC

(A) FG-labeled neurons in the MS (left, upper panel) following tracer injection into the MEC. PV staining of the same section (left, lower panel). The overlay is shown at higher magnification (right panel). Scale bar, 100 μm. Higher magnification images below show the double-labeled neuron indicated by the arrow in the right panel. Scale bar, 20 μm.

(B) FG-labeled neurons in the MS (left, upper panel) following tracer injection into the MEC. CB staining of the same section (left, lower panel). The overlay is shown at higher magnification (right panel). Scale bar, 100 μm. Higher magnification images below show the double-labeled neuron indicated by the arrow in the right panel. Scale bar, 20 μm.

(C) Image of a $FG^+/CTB^+/PV^+$ neuron in the MS following FG (blue) injection into the hippocampus and CTB (red) injection into the MEC. Scale bar, 20 μm.

(D) Image of a $FG^+/CTB^+/CB^+$ neuron in the MS following FG injection into the hippocampus and CTB injection into the MEC. Scale bar, 20 μm.

Abbreviations are as follows: CB, calbindin; CTB, cholera toxin subunit B; FG, fluorogold; HC, hippocampus; MEC, medial entorhinal cortex; MS, medial septum; and PV, parvalbumin.

morphological variance was reported in another study (Gatome et al., 2010). Finally, Canto and Witter (2012) reported that "sag" and "non-sag neurons" comprise at least five cell types when separated on morphological grounds. We searched for additional intrinsic parameters that would help to classify the different cell types in LII. While some parameters were clearly overlapping, we found that the sag, latency to first spike, dAP, and the ratio of ISI1/2 allowed a classification into four cell types. Thus, our analysis enabled us to further subdivide what was formerly denoted as "sag neurons" into stellate, intermediate stellate, and intermediate pyramidal cells. The most conspicuous parameters that helped to distinguish stellate cells from the two intermediate cell types are dAP, latency to spike firing, the initial burst, and the presence of an apical dendrite. Post hoc marker expression analysis of biocytin-filled cells helped to distinguish stellate and intermediate stellate cells from pyramidal and intermediate pyramidal cells in LII. It must be pointed out, however, that we detected co-expression of the two markers both in some intermediate stellate and some intermediate pyramidal neurons.

LII excitatory neurons can be distinguished based on their cell-type-specific excitatory and inhibitory connectivity. Thus, we detected excitatory connections between intermediate cell types that target directly stellate or pyramidal cells, but not between pairs of stellate cells or pyramidal cells. Previous studies emphasized the absence of excitatory connectivity in LII neurons, but concentrated on stellate cells (Couey et al., 2013) or cells with stellate-like appearance (Dhillon and Jones, 2000). The frequency of excitatory connections ranged from 4.3% (between stellate cells to intermediate stellate cells) to 10% (between intermediate pyramidal cells to stellate cells) and is comparable to what was reported for superficial layers in other brain areas (Feldmeyer et al., 2006; Holmgren et al., 2003; Mason et al., 1991).

The importance of inhibition in LII was emphasized by Couey et al. (2013), who highlighted the frequent coupling between FS interneurons and stellate cells. Strikingly, we found here that pyramidal cells were not inhibited either by FS or SOM^+ interneurons, but exhibited recurrent connectivity with $5\text{-}HT_{3A}^+$ interneurons. Cell-type-specific inhibitory connectivity in LII clearly separates pyramidal neurons not only from stellate and

intermediate stellate cells but also from intermediate pyramidal cells. It is safe to assume that the connectivity between 5-HT_{3A}^+ interneurons and pyramidal cells is identical to that reported by Varga et al. (2010). The authors reported that excitatory CB^+, but not RE^+ neurons, are inhibited by cholecystokinin$^+$ basket cells, known to be putative the 5-HT_{3A}^+ interneurons (Morales and Bloom, 1997). Of note, 5-HT_{3A}^+ interneuron connectivity with excitatory neurons in LII also supports the notion that stellate and intermediate stellate cells are distinct neuronal entities.

The presence of four excitatory cell types in LII raises the question as to their function in vivo. The cell-type-specific inhibitory pattern reported here allows the following conjecture. Since there is evidence that activation of FS cells in vivo inhibits grid cell firing most likely via monosynaptic connectivity (Buetfering et al., 2014), and given that FS interneurons inhibit stellate cells, intermediate stellate cells, and intermediate pyramidal cells, we infer that, at least based on the in vitro data reported here, all three cell types fulfill the criteria of putative grid cells. Furthermore, as pyramidal cells do not receive inhibition from FS interneurons, we suggest that grid cells that were identified based on marker expression (Sun et al., 2015; Tang et al., 2014) or morphology (Domnisoru et al., 2013) are very likely the here described intermediate pyramidal cells.

External Input to LII Neurons

We show here that LII neurons receive excitatory input from CB^+ neurons located in the contralateral MEC and inhibitory input from septal long-range GABAergic neurons. Whereas the former excites glutamatergic cells and FS cells, the latter inhibits selectively GABAergic neurons. Needless to say, there are other projections that might be a source of excitation for LII neurons. These, however, were not considered in this study.

On the basis of previous retrograde tracing studies, it could be inferred that LIII neurons project to the contralateral MEC (Amaral et al., 1984; Steward and Scoville, 1976). On the basis of tracing and electrophysiological experiments, we provide evidence that CB^+/$WFS1^+$ neurons in LII are an important source of excitation for contralateral LII neurons. The contralateral projecting CB^+/$WFS1^+$ are very likely identical to the CB^+ cells described by Varga et al. (2010). In the target area all major cell types were excited either directly or indirectly by axons of contralateral CB^+ neurons. This promiscuous targeting in conjunction with the local excitatory connectivity accounts for the high probability of detecting cells in LII that exhibit either monosynaptic or polysynaptic responses upon optogenetic axonal stimulation of contralateral CB^+ projections.

As indicated above, CB^+ cells in LII form island-like structures that do not comprise, however, a homogenous cell population. Thus, not only are the islands composed of pyramidal cells and intermediate pyramidal cells with distinct electrophysiological features, but CB^+ island cells target also different downstream areas, namely the contralateral MEC and the MS. At least based on anterograde and retrograde tracing experiments, we could not detect CB^+ neurons targeting the CA1 region as previously reported by Kitamura et al. (2014), who detected such a projection in transgenic mice.

The reciprocal GABAergic septal-MEC circuit that we identified can be viewed as the pendant of the septal-hippocampal inhibitory pathway. Freund (1989) and Freund and Antal (1988) reported that septal PV^+ cells project to the hippocampus where they target GABAergic neurons; they also described reciprocal connections linking these two brain structures (Takács et al., 2008; Tóth et al., 1993).

Long-range reciprocal GABAergic connections were also found between the hippocampus and the MEC (Melzer et al., 2012). Here we demonstrate that in the MEC, long-range septal GABAergic neurons target exclusively inhibitory neurons. Thus, there is increasing evidence that long-range GABAergic projections constitute a source of disinhibition in the target area.

For decades the septum has been considered the pacemaker of hippocampal and medial entorhinal cortical theta activity, thereby coordinating synchronous activity between distant brain areas (Buzsáki, 2002). In both brain regions distinct cell types fire at a preferred phase of the theta cycle (Mizuseki et al., 2009). Thus, lesions or pharmacological inactivation of the MS strongly reduce theta oscillations both in the hippocampus and the MEC (Jeffery et al., 1995; Mitchell et al., 1982; Petsche et al., 1962), leading to spatial memory deficits akin to those observed after hippocampal lesions (Bannerman et al., 2004; Winson, 1978). At least for the hippocampus, there are several reports directly linking the activity of PV^+ cells in the septum with hippocampal theta activity that results from rhythmic disinhibition (Hangya et al., 2009). A similar mechanism may apply for the MEC. We identified here two distinct sources of GABAergic inputs to the MEC that are ideally suited to synchronize downstream target networks. Of note, from the connectivity pattern it can be concluded that both GABAergic septal projections cause disinhibition in the target area; however, differences in either the recruited networks or their timing is likely, given that the two projections differ with respect to their target cells: septal PV^+ cells inhibit preferentially FS neurons in the MEC, while septal CB^+ neurons inhibit LTS neurons.

Septal input to the MEC also controls the periodicity of grid cell firing as revealed experimentally upon pharmacological inactivation of the septum (Brandon et al., 2011; Koenig et al., 2011). However, so far it is not clear what exactly the contribution of the septal cholinergic is versus the septal GABAergic input to the MEC for the generation of grid cell firing and periodicity.

Conclusions

Our study led to the following main findings, each opening up new avenues that prompt further experimental and theoretical considerations. First, we identified four types of excitatory neurons in LII. Second, the distinct cell types exhibit cell-type-specific excitatory and inhibitory local connectivity. These local networks would meet requirements as proposed by current continuous attractor models for grid cells. Third, we demonstrate that CB^+ neuron activation in LII leads to fast excitation of all major neuronal cell types in the contralateral LII. Finally, we show that the septum disinhibits neurons in LII via two distinct long-range GABAergic projections that exhibit cell-type-specific target selectivity. The exact role of these external sources of direct and indirect excitation for spatial firing and rhythmicity in the MEC warrants further investigations.

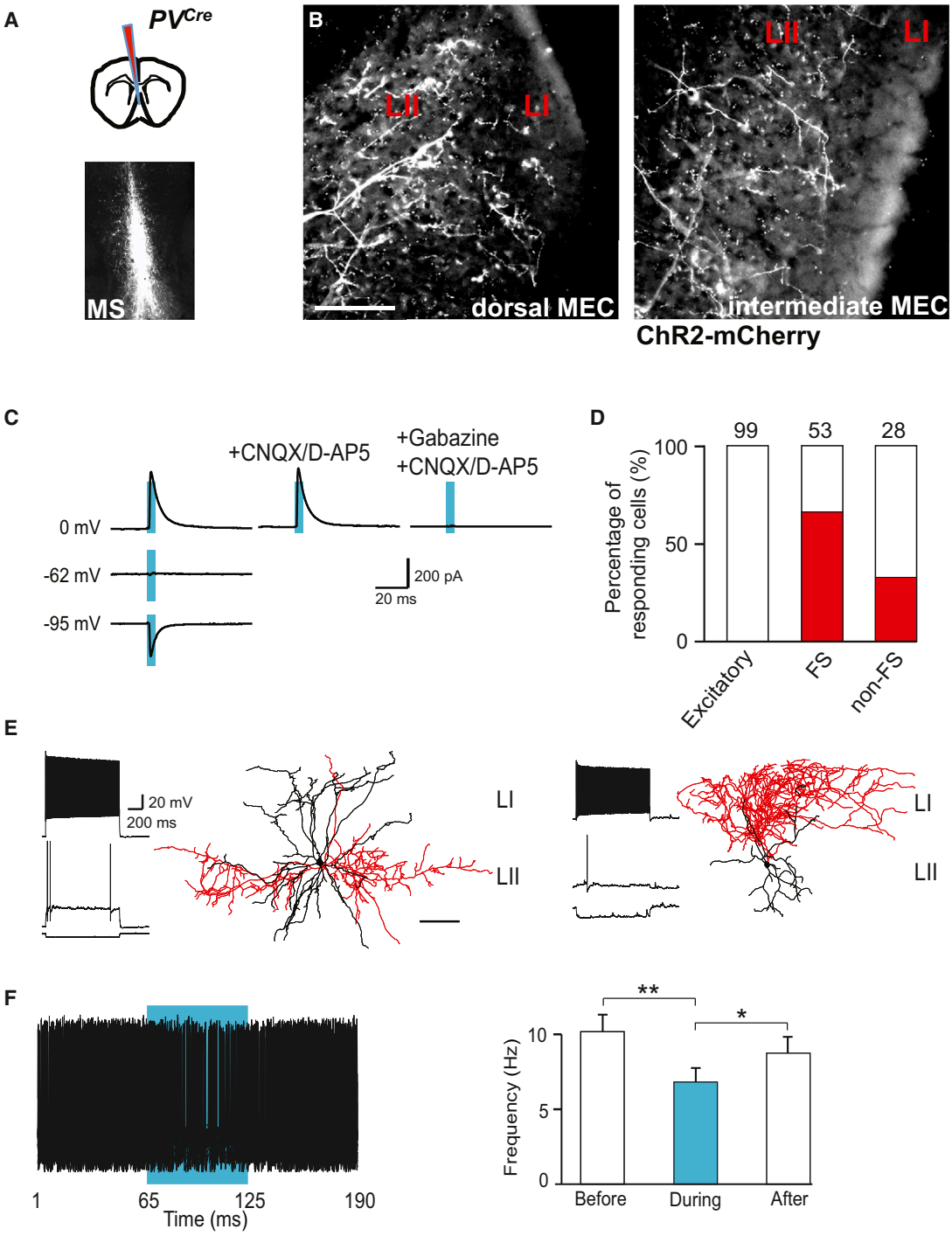

Figure 7. Septal PV^{+} Neurons Inhibit Preferentially FS Interneurons in LII of the MEC

(A) Schematic drawing indicating the site of virus injection into the MS (top). MCherry expression following AAV DIO ChR2-mCherry injection into the MS of a *PV*^{Cre} mouse (coronal section; bottom).

(B) ChR2-mCherry^{+} axons in LII of the dorsal (left) and intermediate (right) MEC (sagittal sections). Scale bar, 50 μm.

(C) Responses of a targeted FS cell in MEC LII at the indicated potentials and in the presence of indicated antagonists. Blue bars show the duration of laser pulses.

(D) Histogram indicating percentage of responding neurons (red) in LII. The numbers above the bars indicate the number of analyzed cells.

(E) Representative firing pattern and reconstruction of a targeted FS (left) and a targeted non-FS GABAergic neuron (right). Dendrites are indicated in black and axons in red. Scale bar, 100 μm.

(legend continued on next page)

EXPERIMENTAL PROCEDURES

Animals

We used wild-type C57Bl/6, *GAD67*^{EGFP} (Tamamaki et al., 2003), *CB*^{Cre} (purchased from Taconic Biosciences), *Uchl1*^{Cre} (obtained from the Mutant Mouse Regional Resource Center), *PV*^{Cre} (Hippenmeyer et al., 2005), *SOM*^{Cre} (Melzer et al., 2012), and *5-HT*$_{3A}$^{EGFP} (Inta et al., 2008) mice. All procedures involving wild-type and genetical modified mice had ethical approval from the Regierungspräsidium Karlsruhe (AZ 35-9185.81/G-173-12) and (G-254-14).

Injection of Retrograde Tracer into the Mouse Brain

Eight-week-old male wild-type and *GAD67*^{EGFP} mice were injected with 100 nl Cholera Toxin subunit B (Alexa Fluor 488 Conjugate or Alexa Fluor 555 Conjugate, Life Technology GmbH) or injected with 70 nl Fluorogold (0.5%, Fluorochrome). Animals were anesthetized with isoflurane, mounted in a stereotactic apparatus, and kept under isoflurane anesthesia during surgery.

For MEC injections, coordinates were 3.1 mm lateral from the midline, 0.1 mm anterior to the transverse sinus, and 1.8 mm below cortical surface; for dorsal hippocampal, 2.4 mm posterior to bregma, 2.0 mm lateral to the midline, and 1.5 below cortical surface; and for MS, 1 mm anterior to bregma and 4 mm below cortical surface.

Animals were perfused 5 to 12 days after injection and the brains processed with immunohistochemical methods. For details, see the Supplemental Experimental Procedures.

Injection of Recombinant Viruses into the Mouse Brain

We injected 8-week-old mice. Injections were performed as described above. 150 nl of recombinant virus were injected in entorhinal cortex or MS. For details, see the Supplemental Experimental Procedures.

Immunohistochemistry, Cell Identification, and Reconstruction of Biocytin-Labeled cells

These methods involved standard procedures described in the Supplemental Experimental Procedures.

Image Analysis

Confocal images were taken using a Zeiss LSM 700 microscope (Zeiss) from anatomically matched sections spanning the lateral-medial extent of the MEC or the rostro-caudal extent of the MS. Data are presented as mean ± SEM. For details, see the Supplemental Experimental Procedures.

Electrophysiology

Whole-cell recordings were performed at 30°C to 32°C using 300-μm sagittal slices containing the dorsal MEC from mice (6 to 12 weeks old).

For paired recordings, LII cells (from 83 mice) were visually identified, and cell pairs with less than 40-μm distances were patched with low Cl^- potassium-based intracellular solution.

Classification of all cells was done based on different electrophysiological parameters reported by others previously (Alonso and Klink, 1993; Couey et al., 2013; Lee et al., 2010). Electrophysiological parameters for excitatory cells are summarized in Table S1.

Connectivity was tested with 40-Hz trains (10 pulses) with postsynaptic cells voltage clamped either at −70 mV to detect uEPSCs or at −50 mV to obtain uIPSCs. uEPSCs were verified with Gabazine/CNQX (both 10 μM), applied sequentially. uIPSCs were inhibited by Gabazine, but not by prior CNQX bath application.

See the Supplemental Experimental Procedures for long-range MEC-MEC or septal-MEC connection experiments.

SUPPLEMENTAL INFORMATION

Supplemental Information includes Supplemental Experimental Procedures, eight figures, and two tables and can be found with this article online at http://dx.doi.org/10.1016/j.neuron.2015.11.029.

AUTHOR CONTRIBUTIONS

E.C.F. and A.C. performed and analyzed the tracing experiments. A.N., R.P., and S.M. performed and analyzed the electrophysiological experiments. H.M. designed and coordinated the study. H.M. wrote the final manuscript with the input of all co-authors.

ACKNOWLEDGMENTS

We thank I. Preugschat-Gumprecht and R. Hinz for their technical assistance and Dr. T. Holland-Letz for the help with the principal component analysis. This work was supported by a European Research Council grant (GABAcellsAndMemory grant 250047, to H.M.), a German Ministry of Education and Research (BMBF) grant (01GQ1003A to H.M. and E.C.F.), and by DFG (grant MO 432/10-1 to H.M. and as part of the CRC 1134).

Received: August 13, 2014
Revised: October 14, 2015
Accepted: October 30, 2015
Published: December 17, 2015

REFERENCES

Alonso, A., and Klink, R. (1993). Differential electroresponsiveness of stellate and pyramidal-like cells of medial entorhinal cortex layer II. J. Neurophysiol. *70*, 128–143.

Alonso, A., and Köhler, C. (1984). A study of the reciprocal connections between the septum and the entorhinal area using anterograde and retrograde axonal transport methods in the rat brain. J. Comp. Neurol. *225*, 327–343.

Amaral, D.G., Insausti, R., and Cowan, W.M. (1984). The commissural connections of the monkey hippocampal formation. J. Comp. Neurol. *224*, 307–336.

Bannerman, D.M., Yee, B.K., Lemaire, M., Wilbrecht, L., Jarrard, L., Iversen, S.D., Rawlins, J.N., and Good, M.A. (2001). The role of the entorhinal cortex in two forms of spatial learning and memory. Exp. Brain Res. *141*, 281–303.

Bannerman, D.M., Matthews, P., Deacon, R.M., and Rawlins, J.N. (2004). Medial septal lesions mimic effects of both selective dorsal and ventral hippocampal lesions. Behav. Neurosci. *118*, 1033–1041.

Beed, P., Gundlfinger, A., Schneiderbauer, S., Song, J., Böhm, C., Burgalossi, A., Brecht, M., Vida, I., and Schmitz, D. (2013). Inhibitory gradient along the dorsoventral axis in the medial entorhinal cortex. Neuron *79*, 1197–1207.

Borhegyi, Z., Varga, V., Szilágyi, N., Fabo, D., and Freund, T.F. (2004). Phase segregation of medial septal GABAergic neurons during hippocampal theta activity. J. Neurosci. *24*, 8470–8479.

Brandon, M.P., Bogaard, A.R., Libby, C.P., Connerney, M.A., Gupta, K., and Hasselmo, M.E. (2011). Reduction of theta rhythm dissociates grid cell spatial periodicity from directional tuning. Science *332*, 595–599.

Buetfering, C., Allen, K., and Monyer, H. (2014). Parvalbumin interneurons provide grid cell-driven recurrent inhibition in the medial entorhinal cortex. Nat. Neurosci. *17*, 710–718.

Burak, Y. (2014). Spatial coding and attractor dynamics of grid cells in the entorhinal cortex. Curr. Opin. Neurobiol. *25*, 169–175.

(F) Stimulation of septal PV^+ long-range projections reduced spiking in LII FS neurons. Responding cells were depolarized to suprathreshold potentials, and long-range axons were stimulated with 60-ms pulses at 8 Hz. Superimposed traces of a representative cell (left) and histogram (right) showing significant reduction of the firing rate during 60-ms pulses (*$p < 0.05$ and **$p < 0.01$). Data represent mean ± SEM.
Abbreviations are as follows: L, layer; MEC, medial entorhinal cortex; MS, medial septum; FS, fast-spiking interneuron; non-FS, non-fast-spiking interneuron; and PV, parvalbumin. See also Figures S7 and S8.

Burak, Y., and Fiete, I.R. (2009). Accurate path integration in continuous attractor network models of grid cells. PLoS Comput. Biol. *5*, e1000291.

Burgess, N., and O'Keefe, J. (2011). Models of place and grid cell firing and theta rhythmicity. Curr. Opin. Neurobiol. *21*, 734–744.

Buzsáki, G. (2002). Theta oscillations in the hippocampus. Neuron *33*, 325–340.

Canto, C.B., and Witter, M.P. (2012). Cellular properties of principal neurons in the rat entorhinal cortex. II. The medial entorhinal cortex. Hippocampus *22*, 1277–1299.

Caputi, A., Melzer, S., Michael, M., and Monyer, H. (2013). The long and short of GABAergic neurons. Curr. Opin. Neurobiol. *23*, 179–186.

Couey, J.J., Witoelar, A., Zhang, S.J., Zheng, K., Ye, J., Dunn, B., Czajkowski, R., Moser, M.B., Moser, E.I., Roudi, Y., and Witter, M.P. (2013). Recurrent inhibitory circuitry as a mechanism for grid formation. Nat. Neurosci. *16*, 318–324.

Dhillon, A., and Jones, R.S. (2000). Laminar differences in recurrent excitatory transmission in the rat entorhinal cortex in vitro. Neuroscience *99*, 413–422.

Domnisoru, C., Kinkhabwala, A.A., and Tank, D.W. (2013). Membrane potential dynamics of grid cells. Nature *495*, 199–204.

Feldmeyer, D., Lübke, J., and Sakmann, B. (2006). Efficacy and connectivity of intracolumnar pairs of layer 2/3 pyramidal cells in the barrel cortex of juvenile rats. J. Physiol. *575*, 583–602.

Freund, T.F. (1989). GABAergic septohippocampal neurons contain parvalbumin. Brain Res. *478*, 375–381.

Freund, T.F., and Antal, M. (1988). GABA-containing neurons in the septum control inhibitory interneurons in the hippocampus. Nature *336*, 170–173.

Gatome, C.W., Slomianka, L., Lipp, H.P., and Amrein, I. (2010). Number estimates of neuronal phenotypes in layer II of the medial entorhinal cortex of rat and mouse. Neuroscience *170*, 156–165.

Giocomo, L.M., Moser, M.B., and Moser, E.I. (2011). Computational models of grid cells. Neuron *71*, 589–603.

Gonzalez-Sulser, A., Parthier, D., Candela, A., McClure, C., Pastoll, H., Garden, D., Sürmeli, G., and Nolan, M.F. (2014). GABAergic projections from the medial septum selectively inhibit interneurons in the medial entorhinal cortex. J. Neurosci. *34*, 16739–16743.

Hafting, T., Fyhn, M., Molden, S., Moser, M.B., and Moser, E.I. (2005). Microstructure of a spatial map in the entorhinal cortex. Nature *436*, 801–806.

Hangya, B., Borhegyi, Z., Szilágyi, N., Freund, T.F., and Varga, V. (2009). GABAergic neurons of the medial septum lead the hippocampal network during theta activity. J. Neurosci. *29*, 8094–8102.

Hippenmeyer, S., Vrieseling, E., Sigrist, M., Portmann, T., Laengle, C., Ladle, D.R., and Arber, S. (2005). A developmental switch in the response of DRG neurons to ETS transcription factor signaling. PLoS Biol. *3*, e159.

Holmgren, C., Harkany, T., Svennenfors, B., and Zilberter, Y. (2003). Pyramidal cell communication within local networks in layer 2/3 of rat neocortex. J. Physiol. *551*, 139–153.

Howard, L.R., Javadi, A.H., Yu, Y., Mill, R.D., Morrison, L.C., Knight, R., Loftus, M.M., Staskute, L., and Spiers, H.J. (2014). The hippocampus and entorhinal cortex encode the path and Euclidean distances to goals during navigation. Curr. Biol. *24*, 1331–1340.

Inta, D., Alfonso, J., von Engelhardt, J., Kreuzberg, M.M., Meyer, A.H., van Hooft, J.A., and Monyer, H. (2008). Neurogenesis and widespread forebrain migration of distinct GABAergic neurons from the postnatal subventricular zone. Proc. Natl. Acad. Sci. USA *105*, 20994–20999.

Jeffery, K.J., Donnett, J.G., and O'Keefe, J. (1995). Medial septal control of theta-correlated unit firing in the entorhinal cortex of awake rats. Neuroreport *6*, 2166–2170.

King, C., Recce, M., and O'Keefe, J. (1998). The rhythmicity of cells of the medial septum/diagonal band of Broca in the awake freely moving rat: relationships with behaviour and hippocampal theta. Eur. J. Neurosci. *10*, 464–477.

Kitamura, T., Pignatelli, M., Suh, J., Kohara, K., Yoshiki, A., Abe, K., and Tonegawa, S. (2014). Island cells control temporal association memory. Science *343*, 896–901.

Klink, R., and Alonso, A. (1997). Morphological characteristics of layer II projection neurons in the rat medial entorhinal cortex. Hippocampus *7*, 571–583.

Koenig, J., Linder, A.N., Leutgeb, J.K., and Leutgeb, S. (2011). The spatial periodicity of grid cells is not sustained during reduced theta oscillations. Science *332*, 592–595.

Köhler, C., Chan-Palay, V., and Wu, J.Y. (1984). Septal neurons containing glutamic acid decarboxylase immunoreactivity project to the hippocampal region in the rat brain. Anat. Embryol. (Berl.) *169*, 41–44.

Lee, S., Hjerling-Leffler, J., Zagha, E., Fishell, G., and Rudy, B. (2010). The largest group of superficial neocortical GABAergic interneurons expresses ionotropic serotonin receptors. J. Neurosci. *30*, 16796–16808.

Li, L.B., Han, L.N., Zhang, Q.J., Sun, Y.N., Wang, Y., Feng, J., Zhang, L., Wang, T., Chen, L., and Liu, J. (2014). The theta-related firing activity of parvalbumin-positive neurons in the medial septum-diagonal band of Broca complex and their response to 5-HT1A receptor stimulation in a rat model of Parkinson's disease. Hippocampus *24*, 326–340.

Mason, A., Nicoll, A., and Stratford, K. (1991). Synaptic transmission between individual pyramidal neurons of the rat visual cortex in vitro. J. Neurosci. *11*, 72–84.

McNaughton, B.L., Battaglia, F.P., Jensen, O., Moser, E.I., and Moser, M.B. (2006). Path integration and the neural basis of the 'cognitive map'. Nat. Rev. Neurosci. *7*, 663–678.

Melzer, S., Michael, M., Caputi, A., Eliava, M., Fuchs, E.C., Whittington, M.A., and Monyer, H. (2012). Long-range-projecting GABAergic neurons modulate inhibition in hippocampus and entorhinal cortex. Science *335*, 1506–1510.

Mitchell, S.J., Rawlins, J.N., Steward, O., and Olton, D.S. (1982). Medial septal area lesions disrupt theta rhythm and cholinergic staining in medial entorhinal cortex and produce impaired radial arm maze behavior in rats. J. Neurosci. *2*, 292–302.

Mizuseki, K., Sirota, A., Pastalkova, E., and Buzsáki, G. (2009). Theta oscillations provide temporal windows for local circuit computation in the entorhinal-hippocampal loop. Neuron *64*, 267–280.

Morales, M., and Bloom, F.E. (1997). The 5-HT3 receptor is present in different subpopulations of GABAergic neurons in the rat telencephalon. J. Neurosci. *17*, 3157–3167.

Pastoll, H., Solanka, L., van Rossum, M.C., and Nolan, M.F. (2013). Feedback inhibition enables θ-nested γ oscillations and grid firing fields. Neuron *77*, 141–154.

Petsche, H., Stumpf, C., and Gogolak, G. (1962). [The significance of the rabbit's septum as a relay station between the midbrain and the hippocampus. I. The control of hippocampus arousal activity by the septum cells]. Electroencephalogr. Clin. Neurophysiol. *14*, 202–211.

Ray, S., Naumann, R., Burgalossi, A., Tang, Q., Schmidt, H., and Brecht, M. (2014). Grid-layout and theta-modulation of layer 2 pyramidal neurons in medial entorhinal cortex. Science *343*, 891–896.

Roudi, Y., and Moser, E.I. (2014). Grid cells in an inhibitory network. Nat. Neurosci. *17*, 639–641.

Steffenach, H.A., Witter, M., Moser, M.B., and Moser, E.I. (2005). Spatial memory in the rat requires the dorsolateral band of the entorhinal cortex. Neuron *45*, 301–313.

Steward, O., and Scoville, S.A. (1976). Cells of origin of entorhinal cortical afferents to the hippocampus and fascia dentata of the rat. J. Comp. Neurol. *169*, 347–370.

Suh, J., Rivest, A.J., Nakashiba, T., Tominaga, T., and Tonegawa, S. (2011). Entorhinal cortex layer III input to the hippocampus is crucial for temporal association memory. Science *334*, 1415–1420.

Sun, C., Kitamura, T., Yamamoto, J., Martin, J., Pignatelli, M., Kitch, L.J., Schnitzer, M.J., and Tonegawa, S. (2015). Distinct speed dependence of entorhinal island and ocean cells, including respective grid cells. Proc. Natl. Acad. Sci. USA *112*, 9466–9471.

Takács, V.T., Freund, T.F., and Gulyás, A.I. (2008). Types and synaptic connections of hippocampal inhibitory neurons reciprocally connected with the medial septum. Eur. J. Neurosci. *28*, 148–164.

Tamamaki, N., Yanagawa, Y., Tomioka, R., Miyazaki, J., Obata, K., and Kaneko, T. (2003). Green fluorescent protein expression and colocalization with calretinin, parvalbumin, and somatostatin in the GAD67-GFP knock-in mouse. J. Comp. Neurol. *467*, 60–79.

Tang, Q., Burgalossi, A., Ebbesen, C.L., Ray, S., Naumann, R., Schmidt, H., Spicher, D., and Brecht, M. (2014). Pyramidal and stellate cell specificity of grid and border representations in layer 2 of medial entorhinal cortex. Neuron *84*, 1191–1197.

Tóth, K., Borhegyi, Z., and Freund, T.F. (1993). Postsynaptic targets of GABAergic hippocampal neurons in the medial septum-diagonal band of broca complex. J. Neurosci. *13*, 3712–3724.

Varga, C., Lee, S.Y., and Soltesz, I. (2010). Target-selective GABAergic control of entorhinal cortex output. Nat. Neurosci. *13*, 822–824.

Winson, J. (1978). Loss of hippocampal theta rhythm results in spatial memory deficit in the rat. Science *201*, 160–163.

Neuron

Supplemental Information

Local and Distant Input Controlling Excitation in Layer II of the Medial Entorhinal Cortex

Elke C. Fuchs, Angela Neitz, Roberta Pinna, Sarah Melzer, Antonio Caputi, and Hannah Monyer

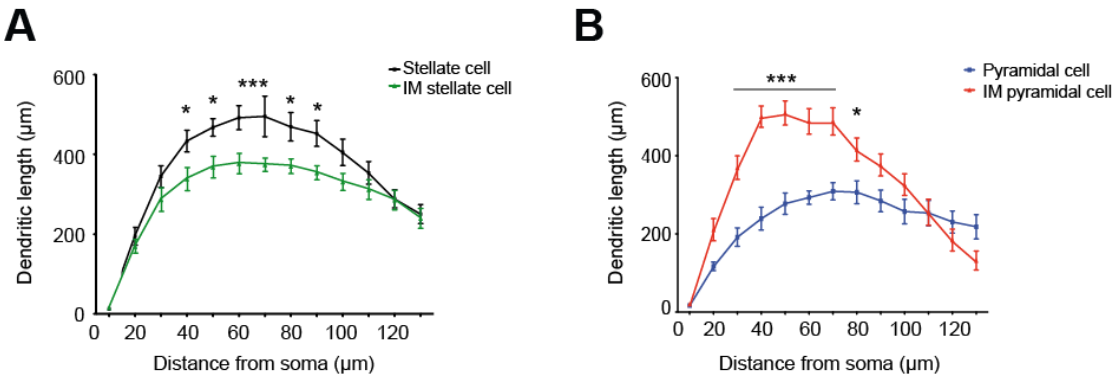

Figure S1. Sholl analysis of dendrites reconstructed from biocytin-filled LII excitatory cells, related to Figure 1

(A) The dendritic density of stellate cells was significantly higher at short distances (40-90 μm) from the soma when compared to that of intermediate stellate cells.

(B) The dendritic density of pyramidal cells was significantly lower at short distances (30-80 μm) from the soma when compared to that of intermediate pyramidal cells (*$p < 0.05$; ***$p < 0.001$, two-way ANOVA followed by post-hoc Bonferroni test). Data represent mean ± SEM. Abbreviations: IM, intermediate.

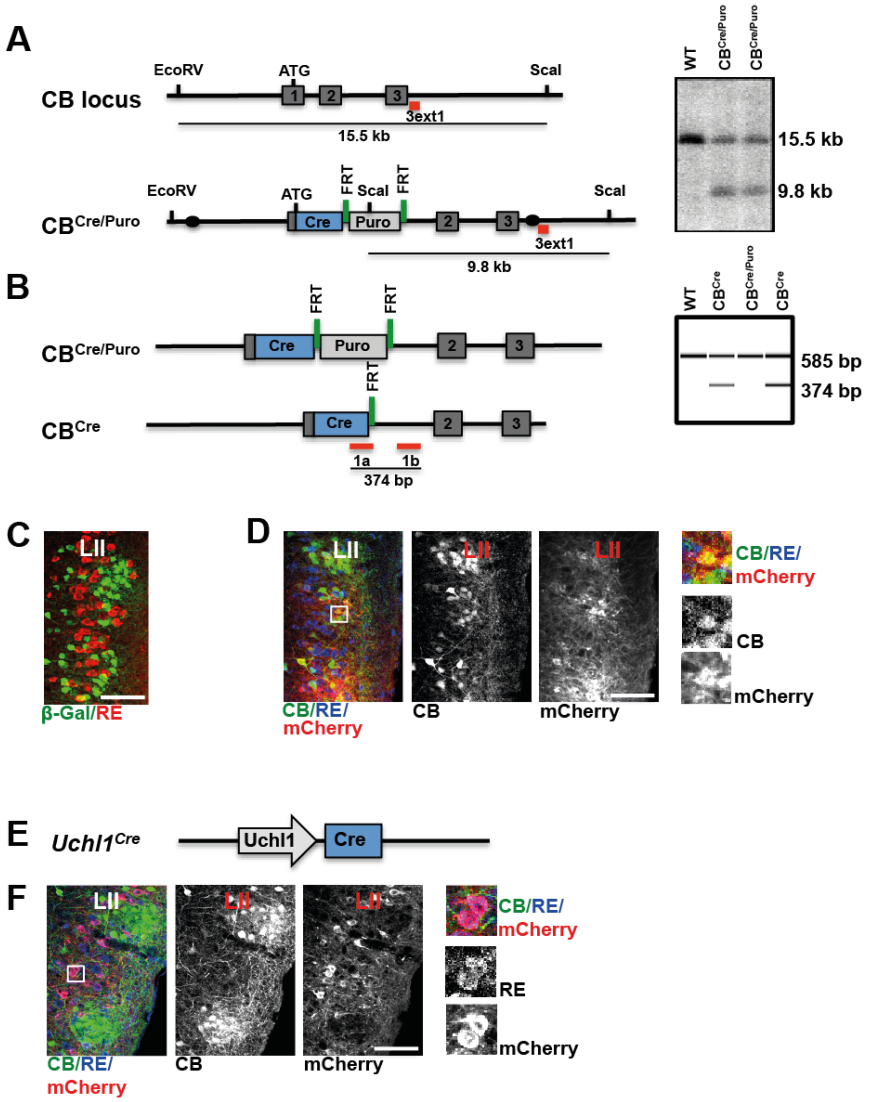

Figure S2. *CB*^{Cre} and *Uchl1*^{Cre} mouse lines used to fluorescently label CB^{+} and RE^{+} neurons in LII, related to Figure 2

(A) Generation of the *CB*^{Cre} mouse via knock-in approach. Schematic representation of gene segments of the wild-type (WT) CB allele and the targeted CB$^{Cre/Puro}$ allele. Dark grey boxes indicate exons, blue box represent Cre recombinase and solid circles indicate the 5' and 3' end of the targeting vector. Positions for EcoRV and ScaI restricition sites are indicated. The green bars stand for the FRT sites flanking the puromycin selection cassette

(Puro). The location of the PCR fragment used as probe for Southern blot analysis is shown as a red bar (left). Southern blot analysis of genomic DNA obtained from WT and $CB^{Cre/Puro}$ ES cells with the 3' external probe demonstrating the presence of a 9.8 kb fragment specific for the modified allele (the 15.5 kb fragment derives from the WT allele; right).

(B) Removal of the puromycin selection cassette after breeding of $CB^{Cre/Puro}$ with FLP deleter mice. The locations of the primer (1a and 1b) used for the demonstration for the removal of puromycin selection cassette are shown as red bars (left). PCR analysis of genomic DNA from WT, $CB^{Cre/Puro}$ and CB^{Cre} mice. The 585 bp control band indicates the presence of genomic DNA and the 374 pb fragment demonstrates the successful removal of the puromycin selection cassette in DNA obtained from CB^{Cre} mice (right).

(C) Crossing CB^{Cre} mice with *ROSA26* reporter mice revealed cell type-specific expression of the reporter gene β-galactosidase in RE^- LII neurons (97 ± 0.6% of β-galactosidase$^+$ neurons were RE^-; 2211 RE^+ and 1434 β-galactosidase$^+$ cells analyzed in 3 CB^{Cre} *x ROSA26* mice).

(D) Confocal picture of immunostaining against CB and RE in LII following AAV DIO ChR2-mCherry injection into the MEC of a CB^{Cre} mouse (left panel). CB staining and mCherry expression of the same section (middle panels). Boxed double-labeled neurons are shown on the right as merged image and the single channels for CB and mCherry. Scale bar, 100 μm.

(E) Schematic drawing showing the transgenic construct used to generate the $Uchl1^{Cre}$ mouse line. Gray arrow represents the *Uchl1* promoter and blue box indicates Cre recombinase.

(F) Confocal picture of immunostaining against CB and RE in LII following AAV DIO ChR2-mCherry injection into the MEC of an *Uchl1*^{Cre} mouse. CB staining and mCherry expression of the same section (middle panels). Boxed double-labeled neurons are shown on the right as merged image and the single channels for RE and mCherry. Scale bar, 100 μm.

Cre recombinase expression in *Uchl1*^{Cre} was restricted to RE^{+} neurons in LII (93.2 ± 2.6% of mCherry^{+} neurons expressed RE; 597 mCherry^{+} and 1272 RE^{+} neurons analyzed in 3 hemispheres from 3 AAV DIO ChR2-mCherry-injected *Uchl1*^{Cre} mice).

Abbrevations: CB, calbindin; Cre, Cre recombinase; β-Gal, β-galactosidase; L, layer; WT, wild-type; Puro, puromycin selection cassette; RE, reelin.

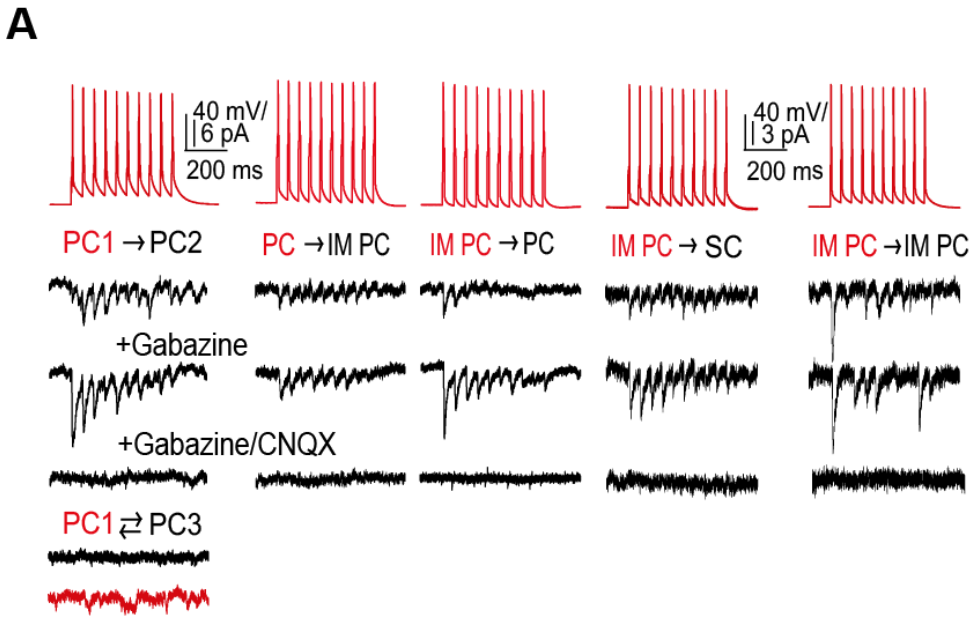
A
40 mV/
6 pA
200 ms
40 mV/
3 pA
200 ms
PC1 → PC2
PC → IM PC
IM PC → PC
IM PC → SC
IM PC → IM PC
+Gabazine
+Gabazine/CNQX
PC1 ⇄ PC3

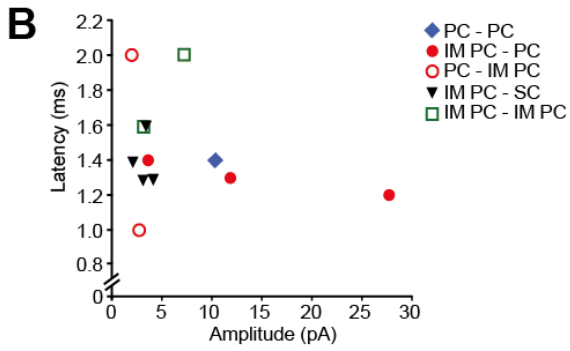
B
PC - PC
IM PC - PC
PC - IM PC
IM PC - SC
IM PC - IM PC
Latency (ms)
Amplitude (pA)

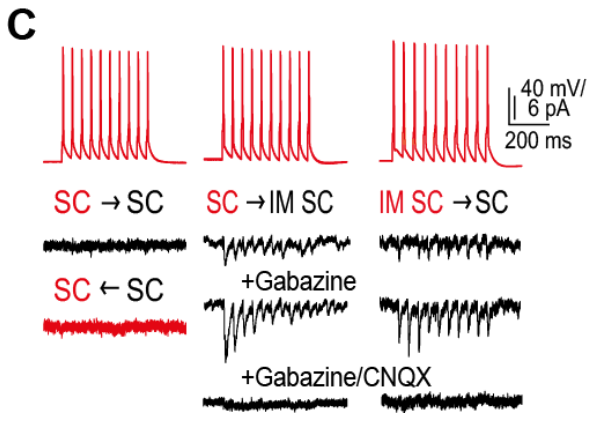
C
40 mV/
6 pA
200 ms
SC → SC
SC → IM SC
IM SC → SC
SC ← SC
+Gabazine
+Gabazine/CNQX

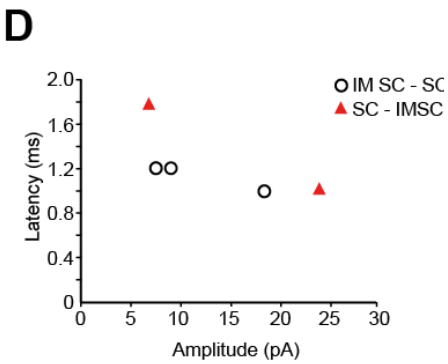
D
IM SC - SC
SC - IMSC
Latency (ms)
Amplitude (pA)

Figure S3. Excitatory connectivity in MEC LII of *CB*^{Cre} and *Uchl1*^{Cre} mice, related to Figure 2

(A) Magnified traces of excitatory cell pairs recorded in *CB*^{Cre} mice, shown in **Figure 2B**, including the single connected PC-PC pair (not shown in **Figure 2;** the neuron termed PC1 was the same presynaptic neuron both for PC2 and PC3). Unitary EPSCs were tested pharmacologically for their excitatory nature. Gabazine and CNQX (both 10 μM), sequentially, but not Gabazine alone, blocked uEPSCs effectively.

(B) Graph depicting averaged peak amplitudes and latencies of the first uEPSCs of all connected LII cell pairs recorded in *CB*^{Cre} mice.

(C) Magnified traces of SC-SC and IM SC-SC cell pairs recorded in *Uchl1*^{Cre} mice, shown in **Figure 2D.**

(D) Graph representing peak amplitudes and latencies of uEPSCs of all connected IM SC-SC cell pairs recorded in *Uchl1*^{Cre} mice.

Abbreviations: PC, pyramidal cell; SC, stellate cell; IM PC, intermediate pyramidal cell; IM SC intermediate stellate cell.

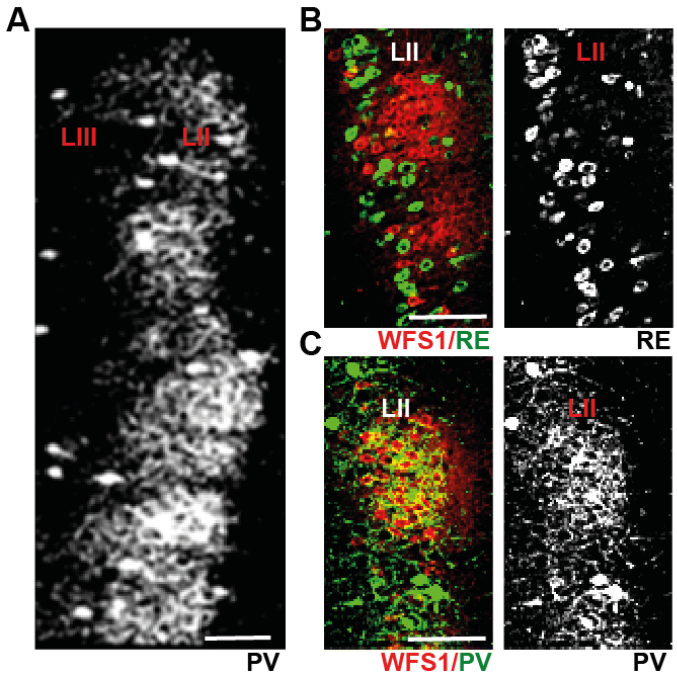

Figure S4. Modular organization of PV$^+$ axons in LII of the MEC, related to Figure 3

(A) PV immunoreactivity in LII of the MEC (sagittal section).

(B) Double-labeling for WFS1 and RE in LII (left), single channel for RE (right).

(C) Double-labeling for WFS1 and PV in LII (left), single channel for PV (right).

Scale bars, 100 μm. Abbreviations: L, layer; PV, parvalbumin; RE, reelin.

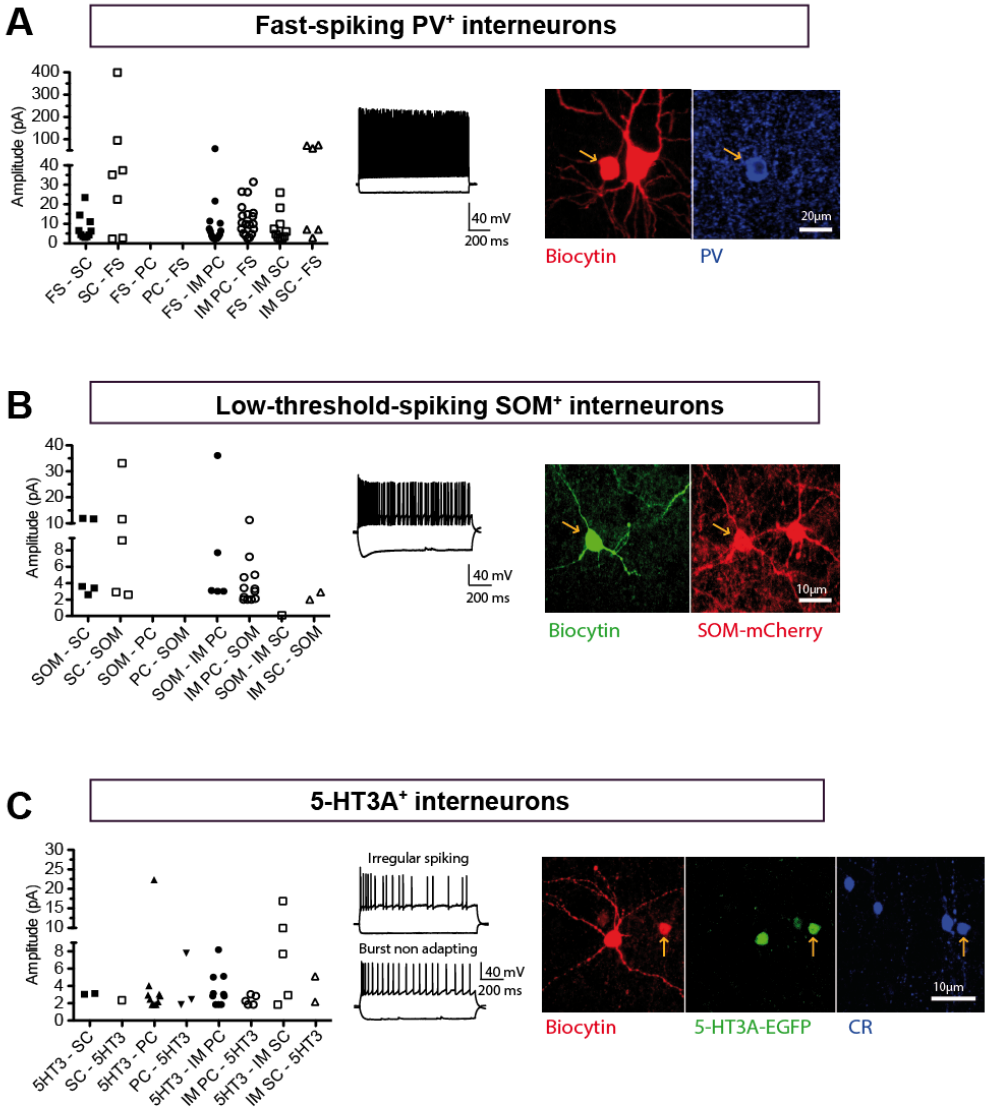

Figure S5. Inhibitory connectivity in MEC LII, related to Figure 3

(A) Graph on the left side represents peak amplitudes of uIPSC and uEPSCs recorded from pairs of FS interneurons and indicated excitatory cells. FS interneurons exhibited a non-adapting spike firing at > 80 Hz, as illustrated in the middle panel, and expressed the Ca^{2+}-binding protein PV (indicated by the yellow arrow in the right panel).

(B) Graph depicting peak amplitudes of uIPSCs and uEPSCs recorded in

pairs of SOM^+ interneurons and indicated excitatory cells. SOM^+ interneurons are characterized by a prominent hyperpolarizing sag, low-threshold firing and spike adaptation, as shown in the middle panel. SOM^+ interneurons in MEC LII of *SOM*^{Cre} mice are labeled with biocytin (green) and express mCherry (red, right panel).

(C) Graph illustrates peak amplitudes of uIPSCs and uEPSCs in pairs of 5-HT_{3A}^{EGFP+} interneurons and indicated excitatory cells. The 5-HT_{3A}^+ interneuron population is a diverse group, including irregular spiking cells (upper middle panel) and burst, non-adapting cells (lower middle panel). Some 5-HT_{3A}^+ interneurons expressed CR (blue; indicated by the yellow arrow in the right panel).

Abbreviations: PC, pyramidal cell; SC, stellate cell; IM PC, intermediate pyramidal cell; IM SC intermediate stellate cell; CR, calretinin; EGFP, enhanced green fluorescent protein; 5-HT_{3A}, 5-HT_{3A} receptor; SOM, somatostatin.

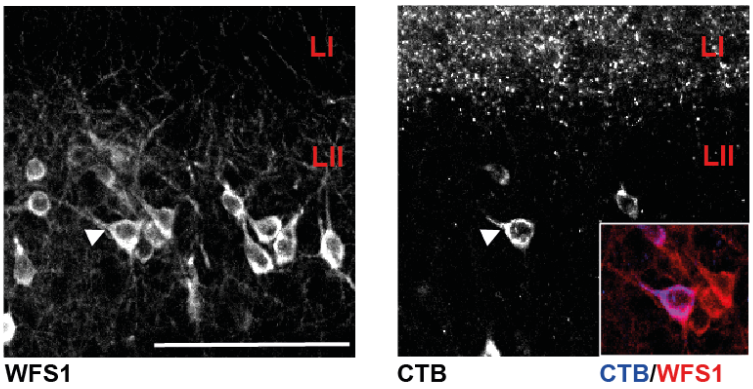

Figure S6. Contralaterally projecting WFS1$^+$ LII neurons, related to Figure 4

Oblique orientation of the main apical dendrite (indicated by white arrowhead) of a WFS1$^+$ (left) and CTB$^+$ (right) neuron in LII. Inset is a higher magnification of the WFS1$^+$/ CTB$^+$ neuron. Scale bar, 100 µm. Abbrevations: L, layer; CTB, Cholera Toxin subunit B.

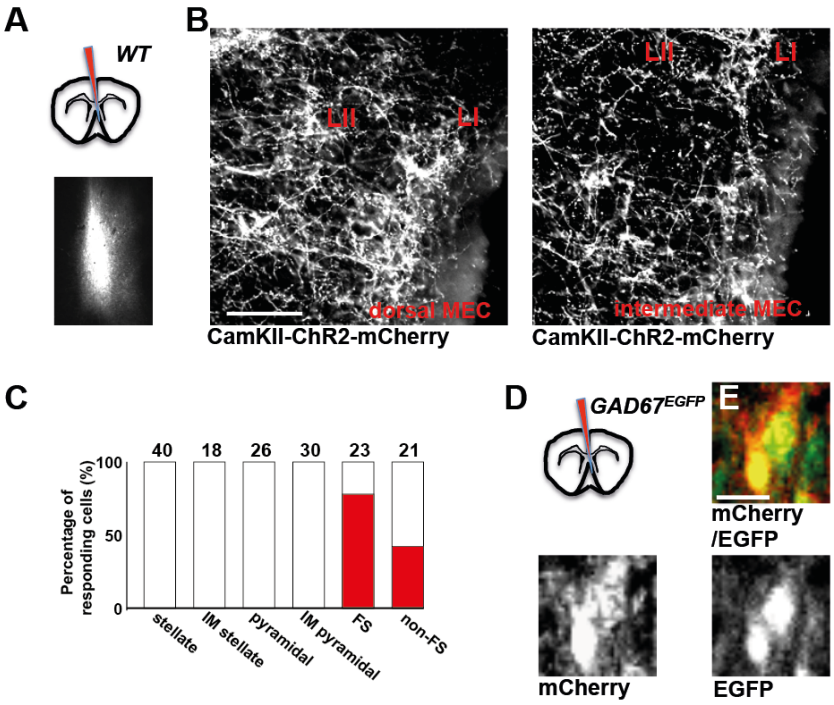

Figure S7. Identification of LII target cells after injection of AAV CamKII ChR2-mCherry into the MS of WT mice, related to Figure 7

(A) Schematic drawing indicating the site of virus injection in the MS (upper panel). MCherry expression following AAV CamKII ChR2-mCherry injection into the MS of a WT mouse (coronal section; lower panel).

(B) ChR2-mCherry^{+} axons in LII of the dorsal (left panel) and intermediate (right panel) MEC (sagittal sections). Scale bar, 50 µm.

(C) Histogram indicating percentage of responding neurons in LII following optogenetic stimulation. Responses could be detected only in FS and non-FS interneurons (red) and were all inhibitory as indicated by the GABAergic reversal potential and the pharmacological blockage with Gabazine, but not with D-AP5 and CNQX (data not shown). Numbers indicate the total number of analyzed neurons (from 16 mice).

(D) Schematic drawing indicating the site of AAV CamKII ChR2-mCherry injection into the MS of a *GAD67*^{EGFP} mouse.

(E) AAV CamKII ChR2-mCherry injection into the MS of *GAD67*^{EGFP} mice demonstrated that expression was not confined to glutamatergic cells, but was also expressed in GABAergic neurons. Co-labeling of mCherry and EGFP (upper panel), single channel for mCherry and EGFP shown in the two lower panels. Scale bar, 10 μm.

Abbreviations: L, layer; ChR2, channelrhodopsin; EGFP, enhanced green fluorescent protein; FS, fast-spiking interneuron; non-FS, non fast-spiking interneuron; IM, intermediate; MEC, medial entorhinal cortex.

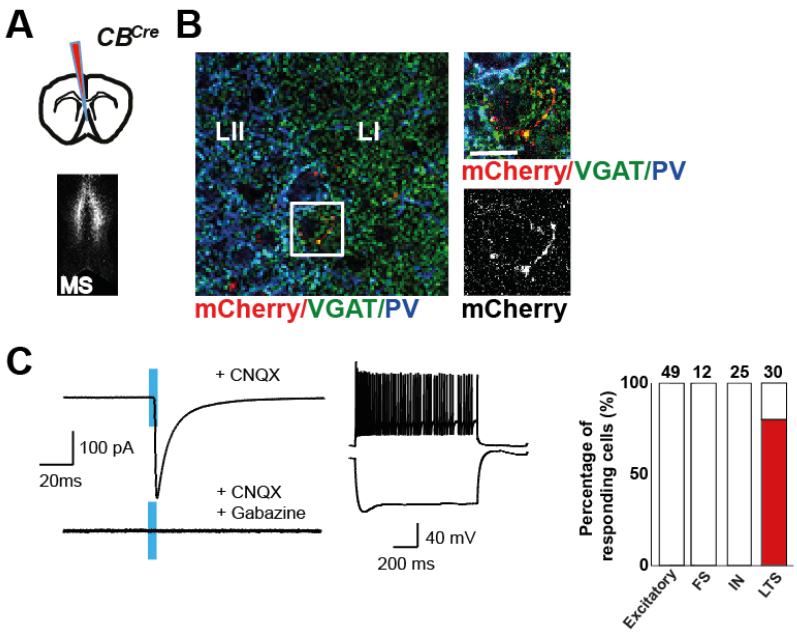

Figure S8. Identification of LII target cells after injection of AAV DIO ChR2-mCherry into the MS of *CB*^{Cre} mice, related to Figure 7

(A) Schematic drawing indicating the site of virus injection in the MS (upper panel). MCherry expression following AAV DIO ChR2-mCherry injection into the MS of a *CB*^{Cre} mouse (coronal section; lower panel).

(B) ChR2-mCherry^{+} axons colocalized with VGAT in the transition zone between LI and LII of the dorsal MEC (sagittal sections). Boxed double-labeled mCherry^{+} axon is shown right (single channel for mCherry in the lower panel). Scale bar, 10 µm.

(C) Synaptic responses and firing pattern of a targeted LTS interneuron, ChR2-mCherry-expressing axons were stimulated by 5 ms laser pulses (blue bar) and IPSCs were recorded. The inhibitory input was identified in the presence of the indicated antagonists. Histogram represents percentage of responding neurons in LII following optogenetic stimulation. Responses were detected only in LTS interneurons (red). IN stands for interneurons, which had

a firing pattern different from FS or LTS interneurons. Total number of analyzed neurons (from 9 mice) is indicated above the bars.

Abbreviations: L, layer; ChR2, channelrhodopsin; CB, calbindin; FS, fast-spiking interneuron; IN, interneuron; LTS, low-threshold-spiking interneuron; MS, medial septum, PV, parvalbumin; VGAT, vesicular GABA transporter.

Cell type	Stellate cells	Pyramidal cells	Intermediate stellate cells	Intermediate pyramidal cells
WFS1/ RE	100 % RE^+ (n = 51 cells)	89.7% $WFS1^+$ 7.6% RE^+ 2.5% $WFS1^+/RE^+$ (n = 39 cells)	73.9% RE^+ 26.1% $WFS1^+/RE^+$ 0% $WFS1^+$ (n = 26 cells)	55.2% $WFS1^+$ 37.9% $WFS1^+/RE^+$ 10.3% RE^+ (n = 36 cells)
V_{rest} (mV)	-65.38 ± 0.33 (#)	-69.98 ± 0.62 (*)	-64.75 ± 0.52 (#)	-67.66 ± 1.20 (#,*)
R_{in} (M**Ω**)	40.73 ± 0.86 (#)	54.02 ± 1.13 (*)	47.72 ± 1.29 (#)	53.08 ± 1.26 (#,*)
sag (mV)	3.73 ± 0.12 (#)	0.11 ± 0.02 (*)	3.77 ± 0.30 (#)	2.06 ± 0.13 (#,*)
Rebound depolarization (mV)	4.52 ± 0.14 (#)	0.56 ± 0.08 (*)	4.22 ± 0.23 (#)	2.52 ± 0.15 (#,*)
latency to spike firing (ms)	23.85 ± 0.70 (#)	206.96 ± 13.74 (*)	350.95 ± 32.55 (#,*)	246.61 ± 22.86 (#,*)
Spike threshold (mV)	-42.23 ± 0.31 (#)	-41.06 ± 0.37 (*)	-42.48 ± 0.48 (*)	-40.75 ± 0.56 (*)
Spike halfwidth (ms)	0.85 ± 0.02 (#)	0.97 ± 0.02 (*)	0.84 ± 0.02 (#)	0.86 ± 0.02 (#)
fAHP (mV)	4.08 ± 0.24	3.83 ± 0.25	5.54 ± 0.31 (#,*)	6.99 ± 0.27 (#,*)
dAP (mV)	2.35 ± 0.09 (#)	0.04 ± 0.008 (*)	1.46 ± 0.11 (#,*)	1.56 ± 0.05 (#,*)
mAHP (mV)	8.39 ± 0.26	9.20 ± 0.26	8.55 ± 0.40	8.90 ± 0.23
ratio of ISI1/ISI2	0.04 ± 0.002 (#)	0.80 ± 0.01 (*)	0.07 ± 0.003 (#,*)	0.70 ± 0.02 (*)

Table S1. Electrophysiological properties of indicated excitatory cells in MEC layer II, related to Figure 1

Characterization of excitatory cell types in MEC layer II of wild type mice, consisting of: (I) stellate cells (n = 128 cells), (II) pyramidal cells (n = 138 cells), (III) intermediate stellate cells (n = 63 cells) and (IV) intermediate pyramidal cells (n = 116 cells). Characteristic electrophysiological properties were analyzed and biocytin-filled cells tested for WFS1- and RE-expression. N equals number of immunostained cells. Abbreviations: RE, reelin; V_{rest}, resting membrane potential; R_{in}, input resistance; fAHP, fast after hyperpolarization amplitude; mAHP, medium after hyperpolarization amplitude; dAP, depolarizing afterpotential; ISI, interspike interval. Data represent mean ± SEM; $p < 0.05$; * significantly different compared to stellate cells; # significantly different compared to pyramidal cells using one-way ANOVA followed by post-hoc Fischer LSD test.

Cell type	Stellate	Intermediate stellate	Intermediate pyramidal	Pyramidal	FS	non-FS
Percentage of responding cells	56 % (n=34)	64 % (n=28)	36 % (n=60)	35 % (n=31)	70 % (n=20)	10 % (n=20)
Number of monosynaptically responding cells	4 (n=13)	1 (n=17)	0 (n=15)	0 (n=8)	1 (n=10)	0 (n=2)
Number of monosynaptic responses blocked by D-AP5/CNQX	4 (n=4)	1 (n=1)	n.d.	n.d.	1 (n=1)	n.d.
Amplitude of monosynaptic response (pA)	14.93 ± 1.77 (n=4)	20.89 (n=1)	n.d.	n.d.	6.12 (n=1)	n.d.
Latency of monosynaptic response (ms)	2.61 ± 0.05 (n=4)	3.89 (n=1)	n.d.	n.d.	3.54 (n=1)	n.d.

Table S2. Responses of LII target cells receiving excitatory input from contralateral CB$^+$ neurons, related to Figure 4

N equals number of recorded cells. Data represent mean ± SEM. Abbreviations: FS, fast-spiking interneuron; non-FS, non fast-spiking interneuron; n.d., not detected.

Supplemental Experimental Procedures

Animals

We used wild-type C57Bl/6, *GAD67*^{EGFP} (Tamamaki et al., 2003), *CB*^{Cre} (purchased from Taconic Biosciences, Cologne, Germany), *Uchl1*^{Cre} (obtained from Mutant Mouse Regional Resource Center, USA), *PV*^{Cre} (Hippenmeyer et al., 2005), *SOM*^{Cre} (Melzer et al., 2012) and *5HT*$_{3A}$^{EGFP} (Inta et al., 2008) mice. All procedures involving wild-type, and genetical modified mice had ethical approval from the Regierungspräsidium Karlsruhe, Germany (AZ 35-9185.81/ G-173-12) and (G-254-14).

Uchl1^{Cre} mice

The mouse strain used for this research project, STOCK Tg(Uchl1-cre)NO63Gsat/Mmucd, identification number 036089-UCD, was obtained from the Mutant Mouse Regional Resource Center, a NCRR-NIH funded strain repository, and was donated to the MMRRC by the NINDS funded GENSAT BAC transgenic project.

Retrograde tracer injection

Eight weeks old male wild-type and *GAD67*^{EGFP} mice were injected with 100 nl Cholera Toxin subunit B (Alexa Fluor 488 Conjugate or Alexa Fluor 555 Conjugate, Life Technology GmbH, Germany), or injected with 70 nl Fluorogold (0.5%, Fluorochrome, Denver, USA). Animals were anesthetized with isoflurane, mounted in a stereotactic apparatus and kept under isoflurane anesthesia during surgery.

For medial entorhinal cortex (MEC) injections, coordinates were 3.1 mm lateral from the midline, 0.1 mm anterior to the transverse sinus and 1.8 mm below the cortical surface. The glass micropipette with a tip resistance of 2 to 4 MΩ was lowered into the cortex with an antero-posterior angle of 6°. The pipette was held in place for 20 min before being retracted from the brain.

For dorsal hippocampal injections a small craniotomy was made 2.4 mm posterior to bregma and 2.0 mm lateral to the midline. Retrograde tracer was delivered through a small durotomy by a glass micropipette with a tip resistance of 2 to 4 MΩ, 1.6 mm below the cortical surface into the dorsal hippocampus.

For medial septum (MS) injections a small craniotomy was made 1 mm anterior to bregma. Retrograde tracer was delivered by a glass micropipette with a tip resistance of 2 to 4 MΩ, 4 mm below the cortical surface into the medial septum.

The scalp incision was sutured, and post-surgery analgesics were given to aid recovery (0.03 mg/kg KG Metamizol). Animals were perfused 5 to 12 days after injection and the brains processed with immunohistochemical methods.

We did not analyze mice in which the injection site did not correspond to the aimed area.

Virus Injections

pAAV-double floxed-hChR2(H134R)-mCherry-WPRE-pA (AAV DIO ChR2-mCherry) vector was obtained from Karl Deisseroth (Cardin et al., 2010). This vector carries an inverted version of Channelrhodopsin 2 fused to the fluorescent marker mCherry. In the presence of Cre recombinase, the

cassette is inverted into the sense direction and the fused proteins are expressed from the EF1 promoter. AAV chimeric vectors (virions containing a 1:1 ratio of AAV1 and AAV2 capsid proteins with AAV2 ITRs) were generated as described (Klugmann et al., 2005). AAV CaMKIIa.hChR2(h134a)-mCherry virus was obtained from Pennvector Core (Penn University, USA).

We injected 8 weeks old male and female *CB^{Cre}*, *Uchl1^{Cre}, PV^{Cre} and SOM^{Cre}* mice with AAV DIO ChR2-mCherry, and wild-type and *GAD67^{EGFP}* mice with AAV CaMKIIa.hChR2(h134a)mCherry.

Animals were anesthetized with isoflurane, mounted in a stereotactic apparatus and kept under isoflurane anesthesia during surgery. Injections were performed as described above. 150 nl of recombinant virus were injected in MEC or MS. We did not analyze mice in which the injection site did not correspond to the aimed area. Immunohistochemical and electrophysiological experiments were done 2-3 weeks after the treatments.

Immunohistochemistry

Mice were transcardially perfused with 4% paraformaldehyde (PFA). Sagittal sections (from MEC) or coronal sections (from MS) were cut at 40 µm thicknesses on a vibratome and washed with phosphate buffered saline (PBS). Free-floating sections were permeabilized and blocked for 2 hrs with PBS containing 5% BSA and 0.2% Triton X-100. The incubation of the sections with primary antibodies was performed for 24 hrs at 4°C. For double-labeling experiments both primary antibodies were incubated at the same time. Sections were washed with PBS and incubated for 2 hrs with Cy3-conjugated secondary antibody (1:1000 Jackson Immunoresearch,

Newmarket, UK) or AlexaFluor488 and Alexa647 secondary antibodies (1:1000; Invitrogen Darmstadt, Germany). After repeated washing with PBS the sections were mounted on 0.1% gelatin-coated glass slides and mounted in Mowiol 40-88. The sections were analyzed by confocal microscopy (Zeiss LSM 700).

Antibodies: Monoclonal anti-calbindin (1:5000, Swant, Bellinzona, Switzerland); polyclonal anti-calbindin (1:5000, Swant, Bellinzona, Switzerland); polyclonal calretinin (1:1000, Swant, Switzerland); polyclonal chicken EGFP (1:1000, Abcam, UK); monoclonal anti-NeuN (1:2000, Millipore, Temecula, CA, USA); monoclonal anti-parvalbumin (1:3000, Millipore, Temecula, CA, USA); monoclonal anti-reelin (1:1000, Millipore, Temecula, CA, USA), polyclonal rat somatostatin (1:1000, Millipore, Temecula, CA); monoclonal anti-VGAT (1:1000, Synaptic Systems, Goettingen, Germany); polyclonal WFS-1 (1:500, Proteintech Group, Inc. Chicago, IL, USA).

Image analysis

Anatomically matched sections were selected, spanning the lateral-medial extent of the MEC or the rostro-caudal extent of the MS. Confocal images were taken using a Zeiss LSM 700 microscope (Zeiss, Jena, Germany). Every third of 40 µm thick sagittal (MEC) or coronal (MS) sections were processed (each 120 µm apart) for each antibody to ensure complete analysis of each cell type across the analyzed brain area.

For quantification of retrogradely labeled neurons, three fields from the medial entorhinal cortex or medial septum (spanning the dorsal-lateral extent

of the section) for each brain section were taken with a 20× objective from a confocal microscope (Zeiss LSM 700). We analyzed seven sections from each animal. Data are presented as mean ± SEM.

Electrophysiology

Slice preparation

Electrophysiological recordings were performed from 6 to 12 weeks old mice. We recorded from acute sagittal slices (300 µm) containing dorsal MEC. The entorhinal and septal injection sites were controlled in horizontal and coronal sections, respectively. Mice were deeply anaesthetized with inhaled isoflurane, followed by transcardially perfusion with ~30 ml ice-cold sucrose solution containing (in mM) 212 sucrose, 26 $NaHCO_3$, 1.25 NaH_2PO_4, 3 KCl, 7 $MgCl_2$, 10 glucose and 0.2 $CaCl_2$, oxygenated with carbogen gas (95% O_2/ 5% CO_2, pH 7.4). Sections were cut in ice-cold oxygenated sucrose solution, followed by incubation in oxygenated extracellular solution containing (in mM) 12.5 NaCl, 2.5 $NaHCO_3$, 0.125 NaH_2PO_4, 0.25 KCl, 2 $CaCl_2$, 1 $MgCl_2$ and 25 glucose. Individual slices were placed in a submerged recording chamber mounted on an upright microscope (Olympus BW-X51) and continuously perfused with oxygenated extracellular solution. Cells in MEC and MS were visualized with DIC optics and epifluorescence was used to detect mCherry fluorescence.

Whole-cell recordings

Whole-cell patch-clamp recordings were performed at 30 to 32°C bath temperature. Recording pipettes were pulled from borosilicate glass

capillaries and had tip resistances of 3-8 MΩ. Liquid junction potentials were not corrected**.** Series resistance was maximally compensated and continuously monitored during the recordings. Cells were discarded if no "Giga seal" was initially obtained or series resistance changed more than 20% or was higher than 40 MΩ. The following intracellular solutions were used: low Cl^- potassium-based solution containing (in mM) 130 K-gluconate, 10 Na-gluconate, 10 Hepes, 10 phosphocreatine, 4 NaCl, 4 Mg-ATP and 0.3 GTP, pH adjusted to 7.2 with KOH. High Cl^- solution containing (in mM) 127.5 KCl, 11 EGTA, 10 Hepes, 1 $CaCl_2$, 2 $MgCl_2$ and 2 Mg-ATP (pH 7.3). Cs^+-based solution containing (in mM) 120 Cs^+-gluconate, 10 CsCl, 10 Hepes, 0.2 EGTA, 8 NaCl, 10 phosphocreatine, 2 Mg-ATP and 0.3 GTP, pH 7.3 adjusted with CsOH. For subsequent morphological and immunocytochemical characterization of patched cells, biocytin (circa 10 mg/ ml; Sigma) was added to the respective intracellular solution.

For paired recordings, layer II cells (from 83 mice) were visually identified and pairs of neurons whose somata were located at a distance of less than 40 µm were patched with low Cl^- potassium-based intracellular solution.

Cells were initially kept in cell-attached mode. After achieving a "Giga seal", whole-cell configuration was established and firing patterns were analyzed in current-clamp mode at resting membrane potential by applying 1 s current pulses, starting from -200 pA in 20 pA steps until maximal firing frequency was reached. Individual traces upon -200 pA current injection, at action potential threshold (for intermediate excitatory cell types) and upon 100 to 600 pA current injection (depending on cell type) were selected for illustration of firing pattern.

Classification of excitatory and inhibitory cells was done based on different electrophysiological parameters reported by others previously (Alonso and Klink, 1993; Couey et al., 2013; Lee et al., 2010). Electrophysiological parameters for excitatory cells are summarized in **Table S1.**

Interneurons were classified according to their typical firing pattern, with PV^+ FS interneurons exhibiting non-adapting firing of action potentials at > 80 Hz, in response to a 600 pA current step, while SOM^+ interneurons displayed a prominent hyperpolarizing sag, low-threshold firing (already at 60 pA current injection) and spike adaptation. The group of 5-HT_{3A}^{EGFP+} interneurons is diverse, consisting of at least 4 distinct interneuron subpopulations in MEC LII. The distinct interneuron subpopulations were identified according to their firing pattern and categorized as previously described by Lee et al. (Lee et al., 2010).

Putative connections were tested with 40 Hz trains (10 pulses) by injection of positive current (800 pA; 1-4 ms; in 10 s intervals) to elicit presynaptic action potentials, while postsynaptic cells were voltage-clamped either at -70 mV to detect uEPSCs or at -50 mV to obtain uIPSCs.

For analysis of possible connections and detection of even small response amplitudes an average of 25 sweeps was used and only stimulus-induced PSCs with a latency of less than 2.4 ms were considered as direct connections. A signal was considered positive only if the signal-to-noise ratio was higher than two. The excitatory connectivity was always verified by using the $GABA_A$ receptor antagonist Gabazine (10 µM; SR 95531 hydrobromide) followed by the AMPA receptor inhibitor CNQX (10 µM), whereas only CNQX had an effect on uEPSCs. Inhibitory connectivity was verified by bath

application of Gabazine, while a previous administration of CNQX (10 μM) did not affected uIPSCs.

For long-range MEC-MEC connection experiments, target cells (from 39 mice) were characterized according to their firing properties in current-clamp configuration as described above. Traces upon -200 pA current injection, at action potential threshold and, in the case of FS interneurons at maximal firing frequency, were selected for illustration of firing pattern. Synaptic inputs were analyzed at a holding potential of -70 mV. EPSCs were recorded in response to 5 ms laser-stimulations (473 nm) using approximately 120 mW/mm^2 laser power. Individual synaptic inputs were tested using the following pharmacological agents: CNQX (10 μM), D-AP5 (50 μM), Gabazine (10 μM), TTX (1 μM) and 4-AP (100 μM), bath-applied.

For septal-MEC connection experiments, cells were patched with high Cl^- intracellular solution and classified based on their firing patterns in current-clamp mode (see MEC-MEC experiments; for illustrations of firing patterns traces upon -50 pA current injection, at AP threshold and maximal firing frequency were selected). Cells were voltage-clamped at -80 mV to analyze PSCs induced by laser-stimulation. In some experiments, cells were first classified with K^+-based intracellular solution and then repatched with Cs^+-based solution to analyze the reversal potential. To test the effect of laser-stimulation onto spontaneous firing, identified targeted fast-spiking cells were patched with K^+-based solution. In these cases, cells were depolarized to suprathreshold potentials in current clamp mode and 31 to 232 sweeps of 3 s duration each were recorded. In the middle of each sweep, long-range projections were stimulated for 1s with 8 Hz laser pulses of 60 ms duration.

All recordings were made using either HEKA PatchMaster EPC 8 or 10 amplifier and signals were filtered at 3 kHz, sampled at 10 or 20 kHz. Data analysis was done offline using HEKA software FitMaster or MatLab (Mathworks). Data are given as mean ± SEM. P-values were calculated with Student's t-test, repeated measures ANOVA and Tukey HSD test in Excel (Microsoft) and SPSS (Version 12.0.1 for Windows). Normal distribution of data was tested with the Kolmogorov-Smirnov test.

Cell identification and reconstruction

Acute slices with biocytin-filled cells in the MEC were fixed overnight in 4% paraformaldehyde, followed by extensive washing with PBS.

For immunocytochemical analysis, acute slices were resliced into 60 µm sections and biocytin-labeling was visualized using streptavidin-Cy3 or streptavidin-Cy2 (both 1:1000, Life Technologies GmBH, Frankfurt, Germany). Subsequent stainings against PV, RE, WFS1 and calretinin were conducted as described in the immunohistochemical section.

For morphological reconstructions, biocytin-filled MEC cells were identified via 3,3'-diaminbenzidine (DAB) staining. Sections were fixed overnight in 4% paraformaldehyde, washed and quenched in 1% H_2O_2 for 5 min. After renewed washing, sections were permeabilized in PBS with 1% Triton X-100 for 1 hr. Subsequently, sections were incubated with avidin-biotin-horseradishperoxidase complex in PBS for 2 hrs at room temperature. Following washing in PBS, sections were developed in DAB and mounted in Mowiol. Labeled cells were reconstructed using the Neurolucida (MBF bioscience, Willston, VT, USA) tracing program. Morphological and Sholl

analysis of reconstructed cells have been performed using Neurotrace (MBF bioscience, Willston, VT, USA). Data are given as mean ± SEM. P-values were calculated with repeated measures ANOVA and Bonferroni post-hoc test using Prism (GraphPad Software, La Jolla, Ca, USA).

A principal component analysis based on the variables sag, spike latency, ISI1/2, dAP and the presence of an apical dendrite was conducted in R (software R version 3.01 and using the function “princomp”). For this purpose all variables were normalized to a standard deviation of 1.

Supplemental References

Alonso, A., and Klink, R. (1993). Differential electroresponsiveness of stellate and pyramidal-like cells of medial entorhinal cortex layer II. J.Neurophysiol. 70, 128-143.

Cardin, J.A., Carlen, M., Meletis, K., Knoblich, U., Zhang, F., Deisseroth, K., Tsai, L.H., and Moore, C.I. (2010). Targeted optogenetic stimulation and recording of neurons in vivo using cell-type-specific expression of Channelrhodopsin-2. Nat. Protocols 5, 247-254.

Couey, J.J., Witoelar, A., Zhang, S.J., Zheng, K., Ye, J., Dunn, B., Czajkowski, R., Moser, M.B., Moser, E.I., Roudi, Y., and Witter, M.P. (2013). Recurrent inhibitory circuitry as a mechanism for grid formation. Nat. Neurosci. 16, 318-324.

Hippenmeyer, S., Vrieseling, E., Sigrist, M., Portmann, T., Laengle, C., Ladle, D.R., and Arber, S. (2005). A developmental switch in the response of DRG neurons to ETS transcription factor signaling. PLoS Biol. 3, e159.

Inta, D., Alfonso, J., von Engelhardt, J., Kreuzberg, M.M., Meyer, A.H., van Hooft, J.A., and Monyer, H. (2008). Neurogenesis and widespread forebrain migration of distinct GABAergic neurons from the postnatal subventricular zone. Proc. Natl. Acad. Sci. U S A 105, 20994-20999.

Klugmann, M., Symes, C.W., Leichtlein, C.B., Klaussner, B.K., Dunning, J., Fong, D., Young, D., and During, M.J. (2005). AAV-mediated hippocampal expression of short and long Homer 1 proteins differentially affect cognition and seizure activity in adult rats. Mol. Cell. Neurosci. 28, 347-360.

Lee, S., Hjerling-Leffler, J., Zagha, E., Fishell, G., and Rudy, B. (2010). The largest group of superficial neocortical GABAergic interneurons expresses ionotropic serotonin receptors. J. Neurosci. 30, 16796-16808.

Melzer, S., Michael, M., Caputi, A., Eliava, M., Fuchs, E.C., Whittington, M.A., and Monyer, H. (2012). Long-range-projecting GABAergic neurons modulate inhibition in hippocampus and entorhinal cortex. Science 335, 1506-1510.

Tamamaki, N., Yanagawa, Y., Tomioka, R., Miyazaki, J.I., Obata, K., and Kaneko, T. (2003). Green fluorescent protein expression and colocalization with calretinin, parvalbumin, and somatostatin in the GAD67-GFP knock-in mouse. J. Comp. Neurol. 467, 60-79.